Soft Matter

PAPER

View Article Online
View Journal | View Issue

Cite this: *Soft Matter*, 2025, **21**, 9303

Remarkable preference for di-substitution in self-assembled glycolipids†

C. Besset,[a] S. Chambert,[a] L. C. Abbott,[b] J. N. Moore,[b] J. W. Goodby,[b] S. J. Cowling *[b] and Y. Queneau *[a]

Lipids are known to be amphitropic, exhibiting lyotropic and/or thermotropic liquid crystal mesophases that can exist between the solid and liquid states of matter. In biological systems, naturally occurring lipids can spontaneously create membraneous structures, which can support the formation of micelles and cells that are the encapsulants for biomaterials. It appears that there is a relationship between the structures of natural lipids, and those of the mesophases that they form, with the most common being lipids having two aliphatic chains attached to a polar head group. These architectures allow for self-organization or self-assembly to occur, thereby supporting the formation of columnar or lamellar structures. In this present study we investigate the stability of lamellar liquid crystal phases as a function of the number of aliphatic chains attached to the polar head groups *via* new glycolipids that we synthesised using click chemistry, and in which triazoles were used to attach the chains to the central sugar scaffolds. Optical microscopy, differential scanning calorimetry and X-ray diffraction were used to study the lamellar liquid crystal behaviour and transition temperatures of these materials; the experimental data indicated that the compound with two chains, derived from trehalose, formed a more ordered lamellar phase than the compounds with one or three chains. DFT calculations gave optimised structures indicating the overall shapes of the isolated molecules. Molecular dynamics simulations enabled us to study the self-assembly of the molecules into lamellar phases. Detailed analyses of these simulations revealed that the molecules with either two or three chains adopted a defined set of folded and extended molecular architectures as the stable lamellar phases formed, providing insight into the relative stability of the phase structure formed by the molecules with two chains.

Received 23rd June 2025,
Accepted 12th November 2025

DOI: 10.1039/d5sm00640f

rsc.li/soft-matter-journal

1. Introduction

It is well-known that thermotropic and lyotropic liquid crystals occur between the solid and liquid states of matter as described in "Introduction to Liquid Crystals: Chemistry and Physics".[1] The first observation of a lyotropic liquid crystal was made by Virchow in 1854[2] for systems composed of myelin in water; myelin is a fatty, insulating substance that surrounds and protects nerve fibers, particularly axons, in the brain and spinal cord. It's crucial for efficient and rapid transmission of nerve impulses, acting like insulation on an electrical wire. Conversely, thermotropic liquid crystals were first reported by Reinitzer in 1888 on the melting behaviour of cholesteryl esters derived from plants.[3] From these eras to today thermotropic liquid crystals have expanded on the materials and electro-optics fronts to become the substances behind the driving force in developments of flat screen displays, amongst many other high technology applications.[4–6]

Since the initial studies on liquid crystals, many other families of bio-materials have been found to be mesomorphic.[7–9] Furthermore, many biological materials are amphiphiles and amphitropic, thereby exhibiting both lyotropic and thermotropic liquid crystal phases. For example, cerebrosides, which are major components of the membranes of neurons, exhibit thermotropic columnar and inverted lyotropic columnar mesophases.[10] In addition, cerebrosides have properties that support cell structures, and are related to diseases such as Gaucher's, Krabbe's, Fabry's, Metachromatic leucodystrophy, and Tay–Sachs ailments.[11] Further, many naturally occurring biological materials which exhibit liquid-crystalline properties can also be the toxic, for instance the glycoalkaloid *solanine*, which can be found in green or sprouted potatoes, can produce

[a] *INSA Lyon, Universite Claude Bernard Lyon 1, CNRS, CPE-Lyon, ICBMS, UMR 5246, Bâtiment Lederer, 1 Rue Victor Grignard, F-69622 Villeurbanne, France. E-mail: bessetceline@gmail.com, stephane.chambert@insa-lyon.fr, yves.queneau@insa-lyon.fr*

[b] *Department of Chemistry, University of York, York, YO10 5DD, UK. E-mail: john.moore@york.ac.uk, john.goodby@york.ac.uk, Stephen.cowling@york.ac.uk, laurence.abbott@york.ac.uk*

† This article is dedicated to the memory of Dr Grahame Mackenzie, whose indefatigable commitment to research and teaching in chemistry has been an inspiration for generations of students and colleagues in the UK and France.

acute poisoning when ingested by humans.[12,13] However, it is not yet clear if there is a direct connection between liquid crystallinity and biological function.

Consequently, it is not surprising that research involving liquid crystals stretches across the breadth of the sciences from physics, chemistry, biology, engineering, to computational modelling and simulations. It even touches unusual areas such as extraterrestrial materials; for example, the following comment made by Dworkin *et al.*[14] that "we investigated the chemical and physical properties of complex organic compounds formed in the laboratory under simulated interstellar conditions. We particularly focused on those properties supporting self-assembly processes, in the presence of water, that are relevant to meteoritic studies and perhaps to the origins of life. We found that complex molecules (amphiphiles) capable of self-assembly are produced by UV photolysis of simple, realistic, interstellar ice analogues". Thus, it appears that lipids can form membraneous structures, on which biological cells are based.

If we examine the architectures of lipids that are found in biological cells it appears these lipids usually possess two rather long, asymmetric fatty-chains attached to a polar, ionic or hydrogen-bonding head group. Furthermore, such structures tend to support the formation of columnar liquid crystal mesophases, whereas lipids with only one chain typically induce the formation of lamellar phases. It is somewhat surprising that lipids, which form columnar structures, are found more commonly in bilayer membranes. In addition, the head groups usually fall into families of phosphates, sugars, and steroids, and combinations thereof.[15]

Given it is possible to have lipids that possess a variety of head groups, to which are attached a number of aliphatic chains limited by the available positions of substitution, we decided to probe the importance of chain number in synthesised lipids. This approach allowed us to control our synthetic methodologies in order to prepare pure and stable materials with defined numbers of aliphatic chains in their chemical architectures. To determine which of the materials prepared possessed the most stable mesophase behaviour their phase transitions were evaluated comparatively, on heating and cooling, by thermal polarized light microscopy,[16,17] differential scanning calorimetry,[18] and X-ray diffraction,[19] and in-depth computational simulations were used to probe the spatial arrangement of the molecules and how their conformations relate to the stability of the mesophase formed.

Given these requirements we chose target systems that were projected to exhibit stable mesophases above room temperature. We chose to prepare materials based on the triazole heterocyclic ring system because as a five-ring system it could possess a maximum of four aliphatic chains. In practice, it was used in substitution patterns for creating mono-, di- and trisaccharidic, amphiphilic, heterocyclic, and glycolipid target materials, **5–8**, that are shown in Fig. 1. The substitutions with aliphatic chains were made using decyl chain lengths, because naturally occurring lipids were usually substituted with aliphatic chains of relatively long length.

The syntheses of the materials were achieved by the use of copper-catalysed cycloaddition between azides[20] and alkynes,[21,22] which is an efficient "click chemistry" reaction that is very useful in many areas of carbohydrate chemistry, thanks to a remarkable chemical stability and biological compatibility.[23,24] The reaction produced carbohydrates grafted with one or more C10-triazole units, which, with respect to stability, can be compared to a C12 ester in terms of the contribution to a lipophilic system.[25] Importantly, glycotriazoles are more robust than glyco-esters; they are less liable to hydrolysis or to degradation on heating than esters,[26] thereby allowing for more reproducible melting investigations with heating and cooling cycles, which allows for accurate studies. Thus, we were able to examine the mesophases that were formed through self-organization as a function of the molecular architecture, which varied the number of alkyl chains and the number and form of the glycotriazole head-groups, and hence the hydrophobic/hydrophilic balance as well as the overall molecular shape.

The use of molecular dynamics (MD) simulations to explore the mesophase structures proved to be challenging, due to these molecules having several component groups that give the possibility of multiple strong inter- and intramolecular interactions, as well as a wide range of possible dynamic molecular structures. In the SI we report the MD methodology and analysis development that we carried out in order to obtain and characterise the mesophases of these systems, since it may be useful more widely for MD studies of glycolipids or other related molecules with complex structures. In the main body of the paper, we report the final set of simulations of the glycolipids we studied here, which gave mesophase types that were comparable to those observed experimentally, as well as providing a rich source of information on the structures of the mesophases and how the dynamic molecular structures self-organise.

2. Experimetal methods

2.1 Synthetic routes

Azido derivatives of methyl glucoside, sucrose, trehalose, and melezitose, all of which are non-reducing sugars were prepared using a methodology previously reported by C. Besset *et al.*[20] 6-Azido-6-deoxy-1-*O*-methyl-α-D-glucopyranoside (**1**), 6-azido-6-deoxysucrose (**2**) 6,6′-diazido-6,6′-dideoxytrehalose (**3**) and 6,6′,6″-triazido-6,6′,6″-trideoxymelezitose (**4**) were reacted with 1-dodecyne to give 1,2,3-triazoles **5**, **6**, **7** and **8**, respectively. Reactions were run in a refluxing H_2O/*tert*-butanol (2 : 1) solution using copper sulfate and sodium ascorbate and the final products **5–8** were obtained in 87% to 92% yields after purification by C_{18} reverse phase chromatography. The four compounds were fully characterized by NMR spectroscopy, notably showing the typical patterns corresponding to the newly formed triazole substituent. Full details of the syntheses and characterizations of all of the materials are given in the SI, including DOSY studies of compound **6** which showed that it gave a similar critical micelle concentration to sodium laurate

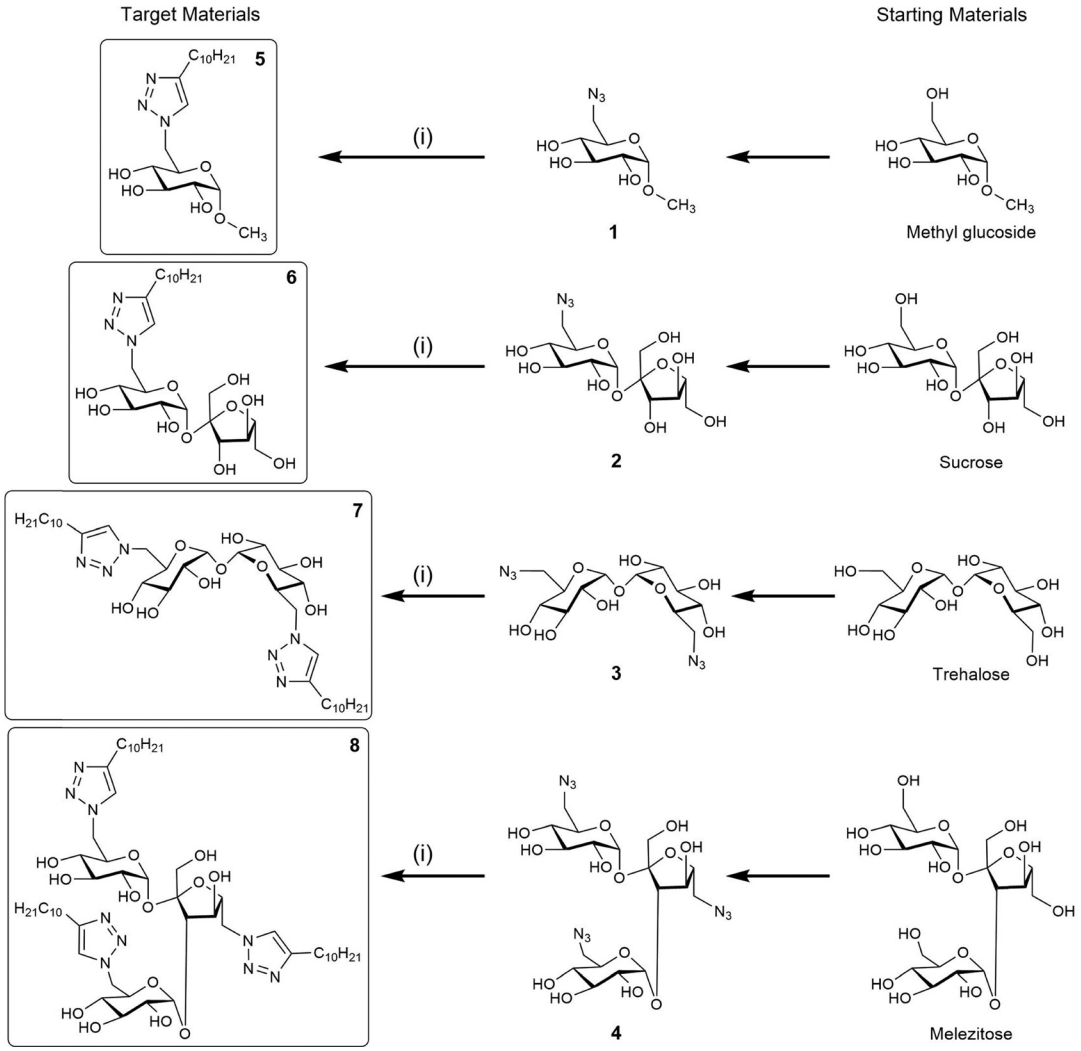

Fig. 1 Structures of the amphiphilic 1,2,3-triazole target materials **5** to **8** comprising flexible decyl aliphatic chain(s), and glycotriazole head groups, and their synthetic pathways starting from methyl glucoside, sucrose, trehalose and melezitose respectively. The reagents and conditions (i) are given as follows: 1-dodecyne (2 equiv.), sodium ascorbate (0.1 equiv.), $CuSO_4$ (0.01 equiv.), H_2O/*t*-BuOH, reflux, 12 h, 87–92%. The intermediate azides are included for completeness and synthetic details for preparation of **1–4** are reported by C. Besset *et al.*[20]

in water, demonstrating that the C10-triazole and C12 ester groups, respectively, have a similar contribution to lipophilic behaviour.

2.2 Characterisation of the mesophase structures and transition temperatures of materials

Thermal polarised optical microscopy is a technique used to observe and identify the optical defect textures of self-organising materials. This technique involves preparing a small amount of a sample on a microscope slide and covering it with a coverslip. The microscope slide is then placed within a heating stage on the microscope. The director field of the sample can orient parallel or perpendicular to the glass surface, which is important for liquid crystal phase classification. For example, a smectic A phase can either give a homeotropic (completely black between crossed polarizers) texture or a focal conic texture for when the molecules are oriented somewhat parallel to the surface of the glass. The combination of textures allows for full classification of the mesophase.[17]

The initial identities of the phases exhibited by compounds **5**, **7** and **8** were made from observing the defect textures formed using thermal polarized optical microscopy (POM) at a magnification of ×100 between crossed polarizers. Differential scanning calorimetry was utilized to confirm the transition temperatures to ±0.5 °C, to determine the melting points recorded on first heating cycles to avoid paramorphosis, and to investigate the temperatures of recrystallization/glassification. X-Ray diffraction studies were performed as a function of temperature with simultaneous collection of small-angle and wide-angle data. The resulting diffraction patterns were collected, radially integrated, and the profiles of the peaks were fitted to give structural information on the phases formed by compounds **5**, **7** and **8**. Full data on the methodologies for the

characterization of the melting behaviour and structural analyses of the mesophases are given in SI.

3. Results and discussion

3.1 Determination of phase types and transition temperatures

Initial studies on the materials by polarized optical microscopy (POM) showed that the melting behaviours were relatively straightforward, with compounds **5**, **7** and **8** exhibiting defect textures consistent with the formation of lamellar phases.[16] The monosaccharide **5** and trisaccharide **8** both gave textures that were predominantly homeotropic, possibly due to the polar, H-bonding sugar moieties strongly interacting with the glass surface of the slides; their defect textures were predominantly optically extinct. However, focal-conic defects at the liquid crystal to air interfaces at the edges of the slide and the cover slip were observed, as shown in Fig. 2(a) for compound **8**. The symmetrical disaccharide, compound **7**, exhibited focal-conic defects possessing elliptical and hyperbolic lines of optical discontinuity,[16,27] in conjunction with homeotropic domains; see Fig. 2(b). The defect patterns observed here are characteristic of the presence of lamellar phases, which for thermotropic phases are of the smectic A type, having either mono-, bi- or interdigitated layer structuring.

Unlike the other materials, compound **6** melted directly into the isotropic liquid and no liquid crystal behaviour was observed even upon rapid cooling of the sample from the liquid in order to facilitate depression of recrystallization. This outcome would seem to be attributable to the compound possessing a disaccharide unit attached to a single aliphatic chain, resulting in the hydrophilic/hydrophobic balance being unfavourable for mesophase formation.

Differential scanning calorimetry was used in combination with POM to validate the transition temperatures observed by POM and also to allow for a direct comparison between the compounds based on their enthalpies of transition. The combined characterization studies on compounds **5**, **7** and **8** gave the transition temperatures and melting points as listed in Table 1 in °C. Interestingly, there was an increase in the melting points as the saccharide and triazole groups increased in number per molecule, but this trend was not observed for the clearing points. The disaccharide **7** exhibited a much higher clearing point than both the monosaccharide **5** and the trisaccharide **8**. The monosaccharide was expected to form a classical lamellar phase where interpenetration of the alkyl chains occurs at the boundary between the layers at one extreme and the polar head groups forming a boundary on the opposing side. This behaviour is consistent with other glycolipids such as octyl β-D-glucopyranoside, the behaviour of which is well documented.[28] The comparatively higher clearing point for disaccharide **7** indicates that the molecules self-organise in a better-ordered way than those of **5**, which may be due to stronger correlations for the in-plane associations with better packing of the molecules, and thereby a relative lowering of the free volume. The trisaccharide **8** exhibits a clearing point that is part way between the clearing points of **5** and **7**. Using a disaccharide such as **7** for illustration, Fig. 3 shows cartoons and associated layers spacings, *d*, for (a) a classical lamellar phase structure and (b) a bilayer lamellar phase structure,

Table 1 Transition temperatures (°C) and enthalpies of the clearing point transitions (kJ mol^{-1}), given in square brackets, for compounds **5**, **7** and **8**

Compound Number	Transition temperatures/°C						
	Cr_1		Cr_2		Lam		Iso liq
5	•	104.9	•	109.8	•	115.1 [1.526]	•
7	•	115.0	—	—	•	215.7 [3.480]	•
8	•	140.0	—	—	•	167.9 [2.347]	•

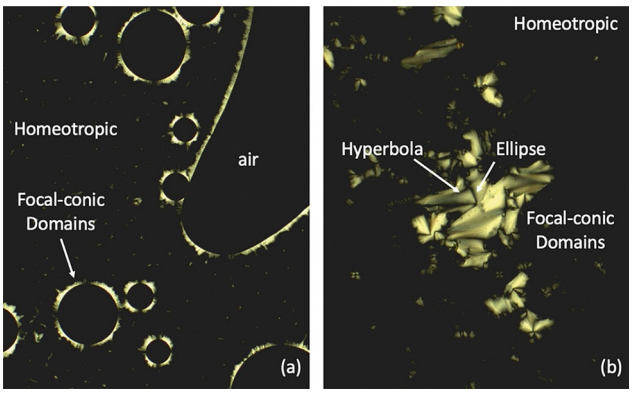

Fig. 2 Photomicrographs (×100 magnification) showing (a) lamellar phase for compound **8** at 160 °C, and (b) focal-conic and homeotropic textures of the lamellar phase of compound **7** at 200 °C. The samples are sandwiched between a microscope slide and coverslip and viewed in transmission mode between crossed polarizers.

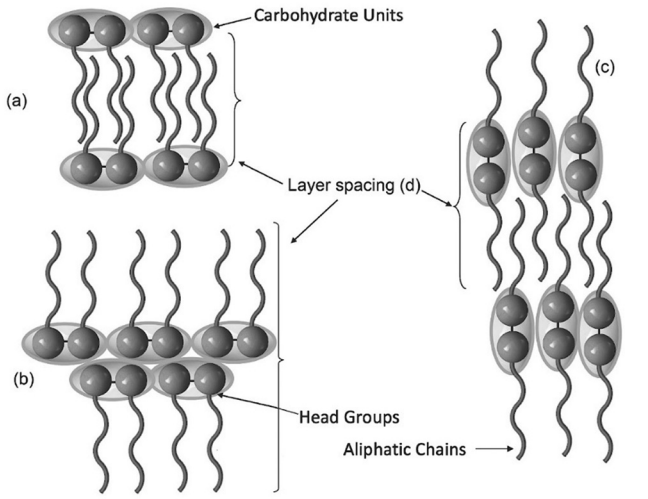

Fig. 3 Cartoon using a disaccharide such as **7** to show (a) a classical lamellar phase structure, (b) a folded dimer lamellar phase structure and (c) an extended dimer lamellar phase structure.

in this case both formed from conformationally folded molecules, and (c) a lamellar phase structure formed from extended molecules. It is not evident from the microscopy and transition temperature data whether the disaccharide **7** (or the trisaccharide **8**) is in a folded or extended conformation. This will be discussed in greater detail in Sections 3.3 and 3.4.

The mesophase behaviour was examined in more detail by differential scanning calorimetry in order to obtain more information about the lamellar phase through peak shape and both enthalpy and entropy of the lamellar to isotropic liquid transitions, as listed in Table 2. The results for the thermal behaviours for the first cooling and second heating DSC cycles of compounds **5**, **7** and **8** are shown in Fig. 4. The initial heating cycles showed broad melting peaks and settling within the sample pan, but cooling and subsequent heating and cooling revealed reproducible phase behaviour, with compound **5** exhibiting numerous crystal to crystal phase transitions. Furthermore, the lamellar to isotropic liquid phase transition temperatures were comparable with the results obtained by POM.

The disaccharide **7** (3.480 kJ mol^{-1}) exhibited the largest comparative enthalpy for clearing, which is consistent with the presence of a more ordered lamellar phase than for the monosaccharide **5** (1.526 kJ mol^{-1}) or trisaccharide **8** (2.347 kJ mol^{-1}). This larger enthalpy suggests that the lamellar phase for **7** may have more extensive hydrogen bonding networks or other intermolecular interactions and/or more cohesive packing of the molecules in the phase than those of **5** or **8**. The enthalpy for the clearing point transition for the trisaccharide **8** (2.347 kJ mol^{-1}) is intermediate between those for **5** and **7**, thereby following the same trend as the transition temperatures. The values for the entropies given in Table 2 exhibit the same trend as the enthalpies and transition temperatures, *i.e.*, **7** > **8** > **5**.

In terms of peak shape, compound **5** shows a typical sharp signal, which indicates a strong, first-order phase transition from the liquid to the lamellar phase, see Fig. 4. However, compound **7** and compound **8** have increasingly broad transition onsets, showing a progression from strong first order character to increasingly more second order on progressing from **5** to **8**.

3.2 DFT calculations of molecular structures

An understanding of 3D molecular shapes forms the basis for understanding the structures of the phases that form by self-assembly. Hence, DFT calculations were carried out using Gaussian 16[29] to model the structures of **5**, **7**, and **8** as isolated molecules. Further details of these calculations are given in the SI.

The large number of intramolecular hydrogen bonds possible within the sugar and triazole moieties of **7** and **8** resulted in a wide range of possible DFT-optimised structures. In the studies reported here, the alkyl chains were generally optimised as all-*trans* conformers, and for **7** two main all-*trans* alkyl chain conformers were examined in detail: a folded conformer and an extended conformer.

Examples of optimised geometries of **5**, **7** and **8** are shown in Fig. 5 in a tubular bond format (left-hand column), and also in a van der Waals surface format with colours used to distinguish the sugar, triazole, alkyl chain, and sugar-to-triazole methylene (CH_2) linking-group moieties. These example structures are discussed below. Total lengths and selected component lengths and widths from these optimised structures are listed in Table 3, and were taken between the edges of the van der Waals surfaces, representing approximate values for these compounds; equivalent distances between atom centres are ≈2.2–3.0 Å shorter than those between van der Waals surfaces, depending on the atom types.

The optimised structure of **5** is somewhat hammer- or wedge-like (Fig. 5) because the cross-sectional area of the head group is larger than that of the all-*trans* alkyl chain. The optimised structure of the folded conformer of **7** is also somewhat wedge-like overall, but less hammer-like than **5** due to the second alkyl chain in **7** providing an infill to the tail shape, with favourable intramolecular dispersion interactions giving near-parallel all-*trans* decyl chains with slight intertwining (partial cooperative twisting) towards the termini (Fig. 5). Calculations that did not include the effects of dispersion resulted in distinctly angular (V-or L-shaped) optimised structures of the folded form of **7**, with the two alkyl chains splayed due to the dominance of repulsive interactions, showing that dispersion effects are likely to be relevant to both intra- and intermolecular interactions between alkyl chains of such compounds in their condensed phases. The optimised structure of the extended conformer of **7** (Fig. 5) corresponds to two parallel but slightly offset rods with a bulbous central connector, arising from the –C–O–C– inter-ring disaccharide connection being perpendicular to the two alkyl chains, and with the structures of the two halves being similar to that of **5**. This extended conformer of **7** was calculated to be ≈60 kJ mol^{-1} higher in energy than the folded conformer of **7**, which may be attributed at least partly to several head-group hydrogen-bonding interactions that were present in the folded conformer but not the extended conformer. In the condensed phase, the extended conformer of **7** may be expected to participate in head-group intermolecular interactions, including hydrogen-bonding interactions, that are not possible for the isolated molecule, such that its energy seems likely to be closer to that of the folded form in condensed phases. The optimised structure of **8** (Fig. 5) is angular, arising from a folded section with some similarity to the folded conformer of **7** plus a slightly protruding outer sugar and its pendant alkyl chain (chain 3). The aligned alkyl chains in the

Table 2 Enthalpy and entropy of the Lam–Iso liq phase transitions. (Universal gas constant R = 8.314 J K^{-1} mol^{-1})

Compound number	Lam–Iso liq T/°C	Lam–Iso liq T/K	ΔH/J mol^{-1}	ΔS/J K^{-1} mol^{-1}	$\Delta S/R$
5	115.1	388.1	1526	3.93	0.47
7	215.7	488.7	3480	7.12	0.86
8	167.9	440.9	2347	5.32	0.64

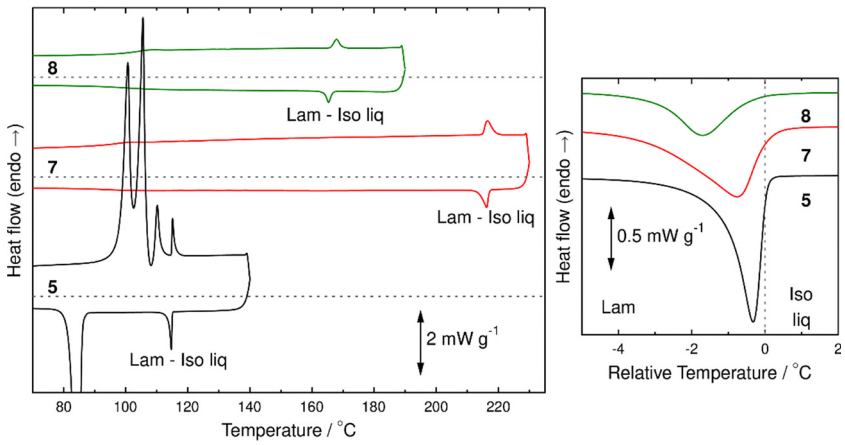

Fig. 4 Left: DSC thermograms (endotherm up) showing the first cooling and second heating processes at 10 °C min^{-1} for compounds **5**, **7**, and **8**, all on the same scale but offset for clarity and with the dashed lines indicating the respective zero heat-flow baselines. Right: An expansion of the isotropic liquid to lamellar transition peaks on first cooling, all on the same heat flow and temperature scales, but offset for clarity and with the relative temperatures set to be 0 °C for 5% of the respective peak height for each compound.

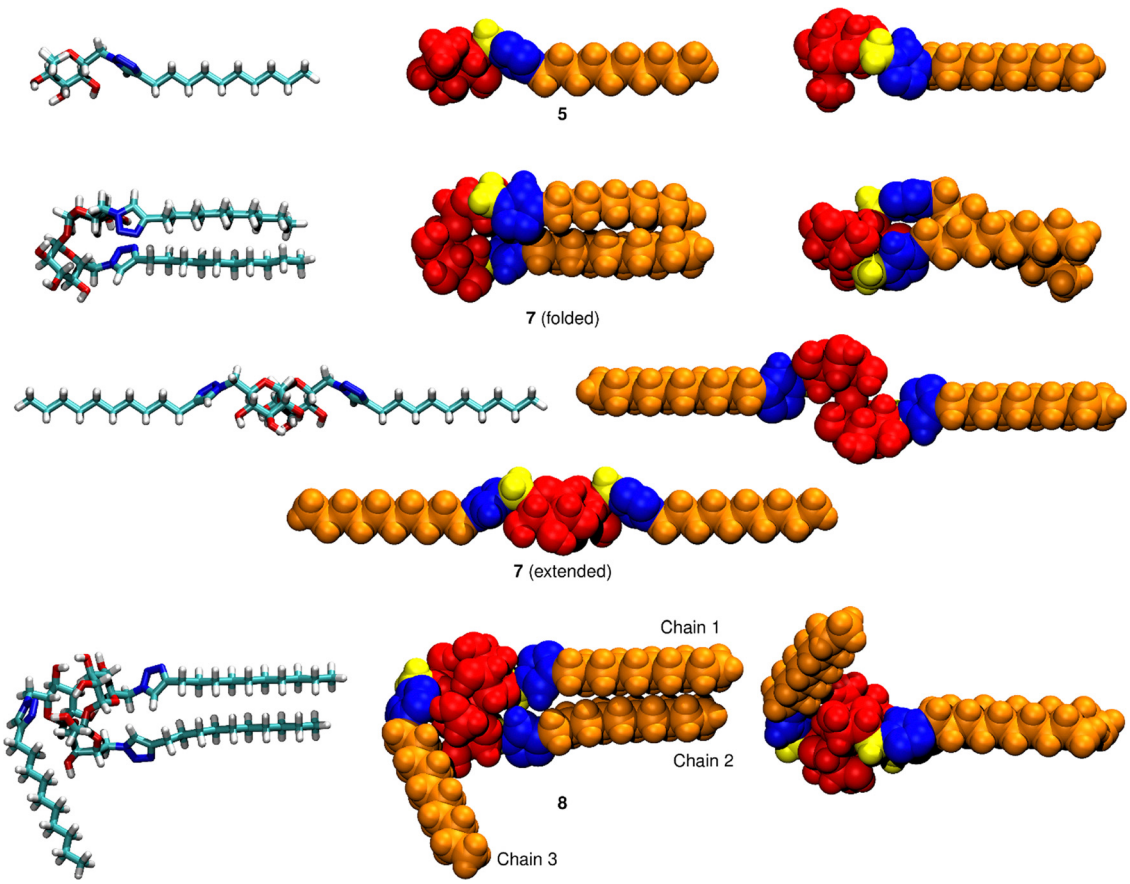

Fig. 5 Examples of optimised structures of **5**, **7** in folded and extended forms, and **8**, determined at the ωB97X-D/cc-pVDZ level of theory. The structures shown as van der Waals surfaces (centre and right-hand columns) are coloured according to moiety types: sugar (red), triazole (blue), alkyl chain (orange), and sugar–triazole methylene (CH_2) linking group (yellow). The left-hand and centre columns show the same orientations, and the right-hand column shows horizontally rotated views.

folded part of **8** are closer and better aligned with each other along their whole lengths than in the folded conformer of **7**, suggesting more favourable intramolecular interactions in **8** than in **7**. The optimised structure of **8** presented here is one example structure, and slightly different intramolecular alkyl-chain dispersion and/or head-group hydrogen-bonding or other

Table 3 A selection of approximate lengths and widths (in brackets) in Å, taken between the edges of van der Waals surfaces from example DFT optimised structures of **5**, **7** and **8** (Fig. 5)

	5		**7** (folded)		**7** (extended)		**8**	
Total	24.4		23.6		42.6		28.6	
Sugar–triazole	10.5	(5.6–8.8)	10.1	(8.9–10.5)	14.6	(9.4–10.4)	10.7	(9.9–10.7)
Alkyl	13.9	(4.7)	13.5[a]	(5.0–9.0)[a]	14.0	(4.7)[b]	13.9[c]	(4.7–7.1)[c]
Sugar	7.7	(5.6–8.8)			8.4	(9.4–10.4)		
Triazole	2.8	(3.4–5.7)			3.1			

[a] For both chains together. [b] For each chain. [c] For both chains 1 and 2 together.

polar interactions are likely to be relevant in other overall geometries that may be possible for an isolated molecule of **8**. As discussed for **7**, condensed phases of **8** will provide the additional possibility of intermolecular interactions of similar types between the various sub-groups. Given the greater number of possibilities for such non-covalent interactions among the three sugars, triazoles and alkyl chains of trisaccharide **8**, it may be expected to have an even wider range of possible structures in condensed phases than disaccharide **7**.

3.3 Phase structure characterization by X-ray diffraction

The structures of the phases of compounds **5**, **7** and **8** were investigated by X-ray diffraction, and all three compounds exhibited simple diffraction patterns that are consistent with lamellar phase structures; example diffraction patterns from compounds **5** and **7** are shown in Fig. 6(a) and (b), and additional diffraction patterns, including those from compound **8**, are shown in Fig. S1 (in the SI). Compound **7** exhibits distinct first (100) and second (200) order diffraction peaks (see Fig. 6(b)), indicating that these molecules produce well-organized layers. For compounds **5** and **8**, only the first order (100) diffraction peak is distinct (see Fig. 6(a) for compound **5**), indicating that these molecules produce more weakly correlated lamellar phases; expanded radial integration patterns shown in Fig. S2 reveal weak second order (200) features from compounds **5** and **8** that are much less distinct than that from compound **7**.

All three compounds also exhibited a diffraction peak in the small-angle region in the isotropic liquid several degrees above the clearing point, indicating pre-organization on cooling, or cybotacticity, occurs in the liquid state (which is not observed by DSC or POM). The pre-organization was most evident for monosaccharide **5**, as shown in Fig. 6(c), and it occurred over a successively shorter temperature range for **7** then **8** (as shown in Fig. S1 and S2). The positions of these peaks are close to those from the respective lamellar phases, indicating that the molecules form layer-like assemblies, or domains, in the isotropic liquid, but that the extent to which they form depends on the molecular structure, with **5** forming them more readily than **7** then **8**. The layer spacings d, obtained for all three compounds are shown as a function of reduced temperature in Fig. 7, which includes values above the clearing point, *i.e.* at $(T_c - T) < 0$. In the region of the clearing point, the change in layer spacing with temperature is sharpest for **5**, and broader for **7** then **8**, which is comparable to the trend in the breadths of the onsets in the DSC peaks for these transitions on cooling (Fig. 4).

The layer spacing at the clearing point is 29.3 Å for **5**, 28.7 Å for **7**, and 31.0 Å around the clearing point for **8**, as shown in Fig. 7.

Taking **7** first, the experimental layer spacing of 28.7 Å is 5.1 Å greater than the total length of the van der Waals surface of the DFT-optimised folded structure of **7** with all-*trans* alkyl chains given in Table 3, and 18.5 Å less than twice this length. Hence, an experimental phase structure that is intermediate between the cartoons in Fig. 3(a) and (b) seems plausible if the sample consists of folded molecules of **7**. A direct comparison of the experimental layer spacing with the lengths of the all-*trans* alkyl conformer quoted here implies that such a phase structure would be closer to the cartoon in Fig. 3(a) than Fig. 3(b), but a sample containing alkyl chains other than the

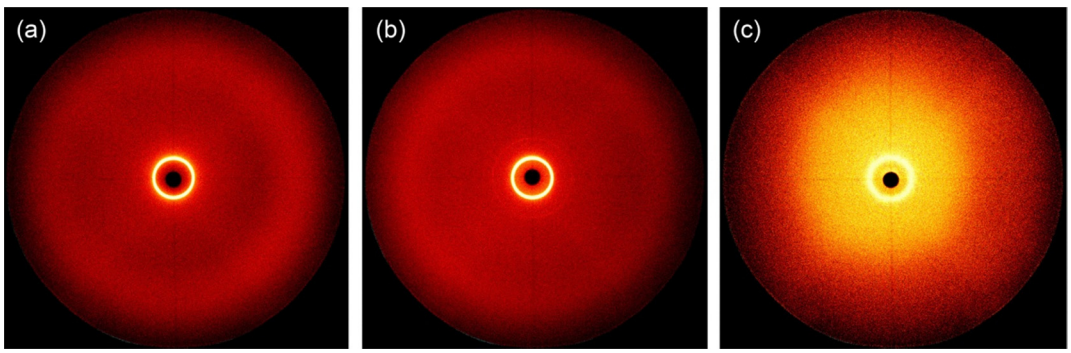

Fig. 6 X-ray diffraction patterns of (a) Compound **5** in the lamellar phase at 110 °C, (b) compound **7** in the lamellar phase showing the 100 and 200 diffraction peaks at 155 °C, and (c) compound **5** in the isotropic liquid phase showing pre-transitional organization at 140 °C.

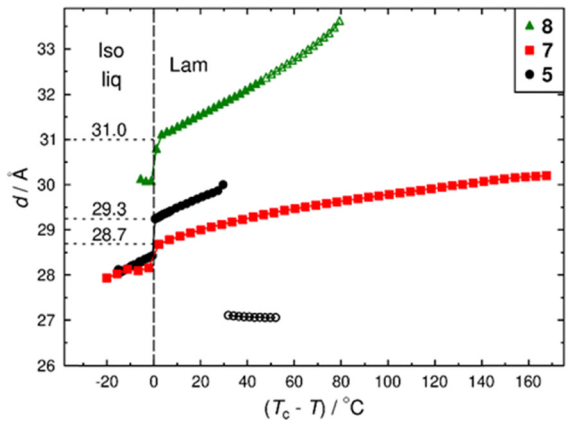

Fig. 7 Layer spacings (d) as a function of reduced temperature ($T_c - T$) for compounds **5**, **7**, and **8**; horizontal dotted lines show the layer spacings at the start of the lamellar phases, and layer spacings within the crystal phases of **5** and **8** are shown by open symbols.

all-*trans* conformer will give shorter molecular lengths and hence a commensurate increase in the ''relative weighting'' of the cartoon in Fig. 3(b) to match the experimental value. The DFT-optimised extended structure of **7** with all-*trans* alkyl chains has lengths of the two halves of the molecule that are comparable to those of the two halves of the folded structure of **7**, such that the total length of the extended structure is less than twice that of the folded structure due to the offset sugars (Fig. 5 and Table 3). Consequently, an experimental phase structure comparable to that in the cartoon in Fig. 3(c) seems plausible if the sample consists of extended molecules of **7**, with the extent of alkyl chain interdigitation relating to the relative composition of all-*trans versus* other alkyl chain conformers, as discussed for the folded molecules of **7**.

A comparable interpretation can be made for the other two compounds. The experimental layer spacings of 29.3 and 31.0 Å for **5** and **8**, respectively, are 4.9 and 2.4 Å greater than the total lengths of the optimised van der Waals structures with all-*trans* alkyl chains given in Table 3, and 19.5 and 26.2 Å less than twice these respective lengths. Hence, experimental phase structures comparable to the cartoons in Fig. 3(a) and (b), with some degree of alkyl chain interdigitation, seem plausible, with the possibility of a phase structure comprising extended structures seeming as plausible for **8** as for **7**.

An examination of Fig. 7 shows that the layer spacing increases with decreasing temperature for all three compounds. On cooling within the lamellar phase, the layers expand by $\approx$0.01 Å °C^{-1} for **7** and by $\approx$0.02–0.03 Å °C^{-1} for **5** and **8**, such that the lamellar layer spacing of **7** has a weaker temperature dependence than those of **5** and **8**.

On cooling, the alkyl chain populations will tend towards lower energy conformers that are more linear and can pack together more tightly. In order to avoid the introduction of void volumes as the tail groups pack more tightly, it seems reasonable to attribute the increase in layer spacing on cooling principally to the head groups moving slightly away from the notional side-to-side arrangements shown by the cartoons in Fig. 3. On cooling, this effect would result in a partial and increasing offset of the head-groups to give entropically favourable packing that minimises the overall free volume but increases the layer spacing. The different temperature dependences of the experimental layer spacings for **5**, **7** and **8** can be attributed to their different molecular and/or phase structures. For **7**, both the folded and extended forms have relatively rod-like structures in which the cross-sectional areas of the respective head- and tail-groups are similar, such that potential void volumes leading to layer expansion may occur less readily than for **5**, which has a less rod-like and more hammer-like shape. In addition, if **7** is present in the extended form, then the out-of-plane phase structure may be maintained over longer distances through interpenetration, as shown in Fig. 3(c), with the possible consequence that the layer spacing might be less affected by temperature. The possible molecular shapes and hence phase structures of **8** are more complex, but similar possibilities to those for **7** also apply.

3.4 Molecular dynamics simulations of phases

Molecular dynamics simulations provide a computational approach to studying phase structures and the self-assembly of molecules to give ordered phases, with fully atomistic simulations enabling the 3D structures of the molecules present within such phases to be explored. Hence, fully atomistic molecular dynamics (MD) simulations were performed on **5**, **7**, and **8** to explore their lamellar phases.

Overview of the MD simulations. A significant set of preliminary MD runs, including those at various temperatures, was carried out in order to determine the conditions for the final set of simulations, which is reported here in the main body of the paper. These final simulations were started from systems that had been pre-equilibrated in lamellar phases, and they were run for 1000 ns at a temperature of 40 K below the clearing point in the respective simulation ($T_{c,sim}$), which corresponded to a reduced temperature of $T/T_{c,sim}$ = 0.925, 0.935 and 0.938 for **5**, **7** and **8**, respectively. Full details of the MD simulation methods are given in the SI, along with results, analyses and discussion arising from the various sets of preliminary simulations that led to the conditions and pre-equilibrated systems used as the starting geometries for the final set of simulations.

The final set of simulations used a simulation box containing 512 molecules, with the simulations having started originally from molecules in a pseudo-lamellar arrangement with their long axes aligned in an 8 × 8 × 8 grid (details in the SI). The simulation boxes for **5** and **7** in the folded form had initially been created with alternating layers of molecules with the alkyl chains pointing ''up'' and ''down'', resulting in a box containing four overall layers, whereas for **7** in the extended form and **8** the boxes had initially been created without such ''up'' and ''down'' alternation, resulting in a taller and narrower box containing eight layers. The simulation boxes had been created with molecules in the optimised structures shown in Fig. 5, apart from the protruding alkyl chain in **8** being rotated slightly so that the three alkyl chains were closer to parallel to facilitate interdigitation at the start of the simulations.

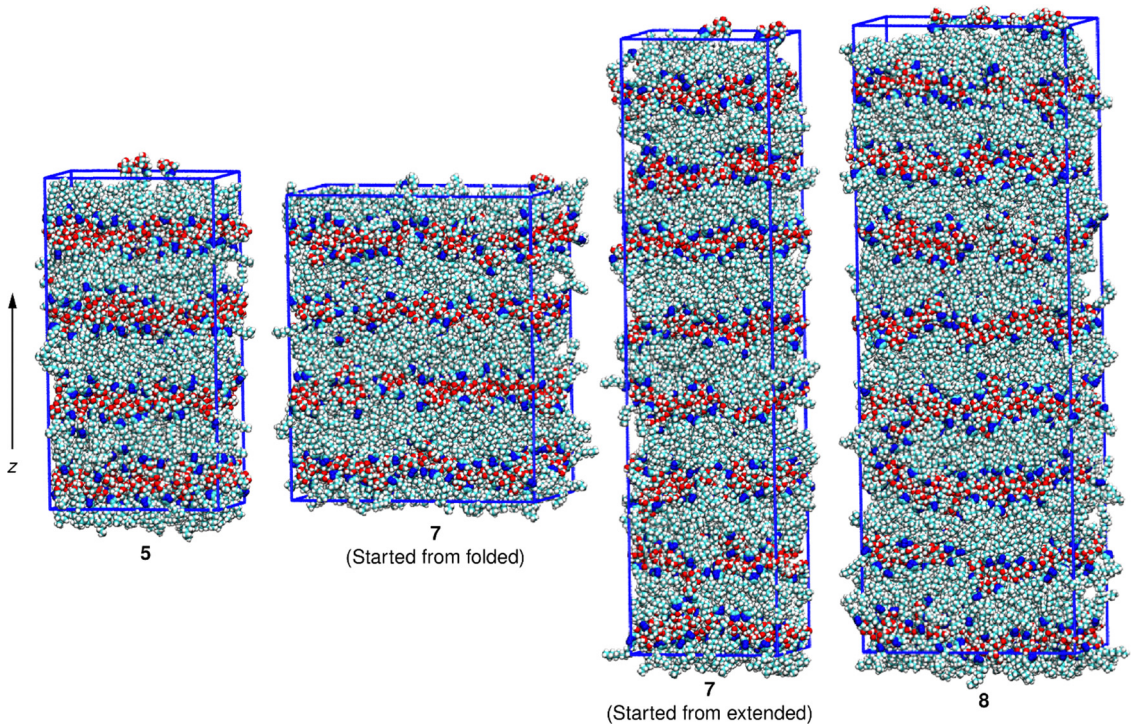

Fig. 8 Example snapshots from MD simulations of **5**, **7** started from the folded form, **7** started from the extended form, and **8**, all run at temperatures of 40 K below the clearing points in the respective simulations and showing the frame at 75 ns during a 1000 ns run. The atom colours match those in the left-hand column of Fig. 5.

The simulations used periodic boundary conditions, and anisotropic pressure coupling that allowed the simulation box aspect ratios and dimensions along all three axes to change freely and independently during the runs, although most stayed close to the starting dimensions and retained the starting number of layers. Fig. 8 shows illustrative snapshots from the final set of simulations; the details of these simulations are presented and discussed below.

An analysis of the MD simulations revealed that the range of molecular structures present in the layered phases differed significantly from the starting molecular structures (Fig. 5) and that the molecules of **7** and **8** were flexible enough for the multiple alkyl chains within a single molecule to behave relatively independently of each other. The independent behaviour of the alkyl chains was considered *via* the schematic representations shown in Fig. 9, where the molecules of **5**, **7** and **8** are represented by a glycotriazole head-group to which one, two or three alkyl tail-groups, respectively, are attached. As shown in Fig. 9, each alkyl chain within a molecule can be labelled "d" or "u" for chains pointing down or up, respectively, in relation to a vertical *z*-axis and a head-group that resides within a horizontal layer, such as the head-group layers shown in Fig. 8. These representations show that there are two possible general forms of **5** (d and u), four possible general forms of **7** (folded forms dd and uu, and extended forms du and ud), and eight possible general forms of **8** (ddd, uuu, ddu, uud, dud, udu, udd and duu), with the respective pairs of down/up forms being related by a horizontal 180° molecular rotation. As an example, ddu corresponds to a molecule with chains 1 and 2 pointing down and chain 3 pointing up from a horizontal layer that contains the sugar of that molecule of **8**, and uud is the paired form that corresponds to the same molecule pointing in the opposite direction along the *z*-axis. The two alkyl chains in **7** are chemically equivalent due to their identical attachments to the disaccharide within the head-group, although they may differ within instantaneous structures. By contrast, the three alkyl chains in **8** are chemically inequivalent due to their different attachments to the trisaccharide within the head group, and with the central saccharide also being structurally different from the other two saccharides (Fig. 1). The specific chain numbering for **8** shown in Fig. 5, and discussed earlier in relation to the DFT-optimised structure, was used consistently. For **7**, the two chains were labelled 1 and 2 for each molecule in a data set, and these labels were then used consistently for the respective chains of that molecule throughout any analyses of that particular data set.

The simulations carried out here resulted in horizontal layers that were spaced along the vertical *z*-axis of the simulation box (Fig. 8). Hence, each molecule within a simulation was readily classified as one of the forms shown in Fig. 9 by inspecting each saccharide core in turn, and using the simple rule that each alkyl chain attached to that core was labelled "u" if its terminal carbon atom was above a defined reference atom within the saccharide core (*i.e.* it had a higher *z* position), otherwise it was labelled "d". The reference atoms were defined as the C2 carbon of the glucopyranose ring for **5**, the central

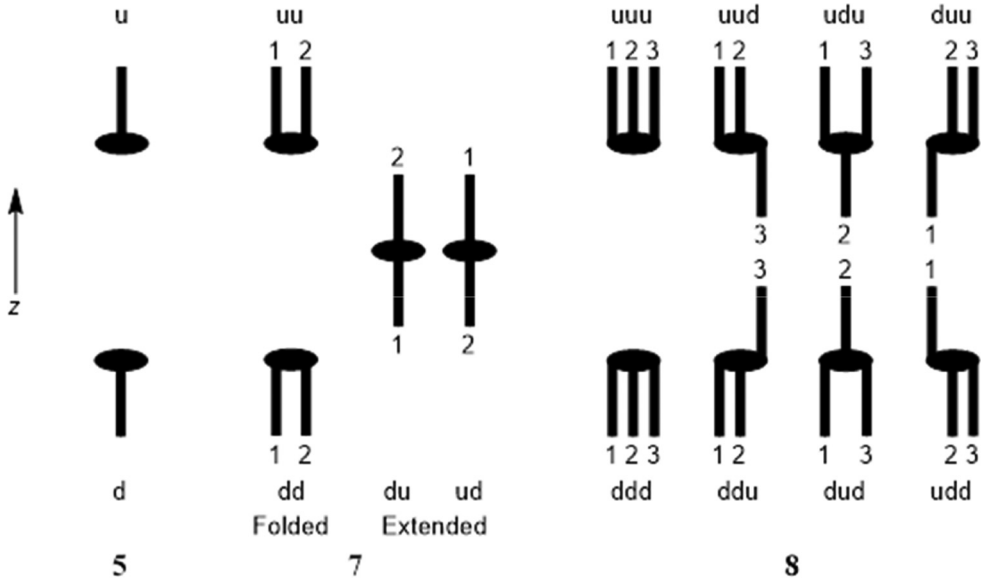

Fig. 9 Schematic representation of the general forms of **5**, **7**, and **8**; the ovals represent the head-groups, the sticks represent numbered alkyl chains that may point independently either down (d) or up (u), and the respective pairs of down/up forms are related by a horizontal 180° molecular rotation. The vertical sticks represent a wide range of possible conformers for each alkyl chain.

oxygen within the glycosydic bond between the two sugar rings for **7**, and the oxygen within the glycosidic bond to the 2-position of the central fructofuranose ring for **8**.

Phase structures in the MD simulations. The fractional populations of the general forms, the positional order parameters, and the layer spacings from the final set of simulations on **5**, **7** and **8** are shown in Fig. 10, along with experimental layer spacings. Each system was fairly unchanged over the course of these 1000 ns runs, apart from some small changes in relative populations of the forms present and some small fluctuations in the layering. The systems that had originally been created with either folded or extended forms of **7** had evolved through the preliminary sets of simulations to give essentially the same fractional populations and phases (details in the SI), such that both the pre-equilibrated starting systems and the results from the final simulations of these two systems were closely similar, as shown in Fig. 10.

An analysis of the fractional populations, taken as averages across the whole 1000 ns simulations, is given in Table 4 as percentages. In all cases, there are as many molecules with chains pointing up as down, within uncertainties of ≈1–2%. The averages for **7** indicate that ≈66% of the molecules are in the folded form (dd or uu) and ≈34% are in the extended form, *i.e.* a ratio of approximately 2 : 1 folded : extended, for systems that started initially from either folded or extended arrangements. The averages for **8** indicate that ≈48% of the molecules are in the "partially folded" form where chains 1 and 2 point in similar directions (ddu and uud), ≈31% are in the "fully folded" form where all three chains point in similar directions (ddd and uuu), ≈11% are in the partially folded form where chains 2 and 3 point in similar directions (udd and duu), and the smallest proportion of ≈10% are in the partially folded form where the two outer chains 1 and 3 point in similar directions and the middle chain 2 points in a different direction (dud and udu). These fractional populations essentially replicate those obtained at similar temperatures during preliminary simulations reported in the SI.

These runs gave phases of **5**, **7** and **8** that were relatively stable and maintained a constant number of layers, but the systems were fluid and dynamic, with molecules changing shape and moving between layers, and with the layers showing some fluctuations. Histograms were constructed to show the normalised populations of selected sets of atom centres along the *z*-axes in the simulations, which correspond to the positions of these atoms within the layers. Selected atom sets were those of the sugar (red), triazole (blue) and alkyl (orange) groups, using all atoms of the respective colour shown in the middle and right-hand columns of Fig. 5, and with the populations being normalised against all of the atoms of each respective atom set in all of the molecules in the simulation. The histograms were made from time-windows of 50 ns, during which any layer fluctuations along the *z*-axis were smaller than such fluctuations across the whole 1000 ns runs, and they included plots of all the molecules (labelled total), and separate plots of each of the general forms of the molecules shown in Fig. 9 (d, u, dd, *etc.*). These histograms may be interpreted with the aid of selected snapshots of single frames from the simulations, using the same colours. Histograms made from a time window of 50–100 ns and selected snapshots of single frames within this time window are shown in Fig. 11–16, with a selection of average histogram peak analysis data given in Table 5. The results are presented and discussed below for **5**, **7** and **8** in turn.

For **5**, the histogram of total populations given at the top of Fig. 11 shows that the sugars (red) form clear layers, that the triazoles (blue) form narrower layers on either side of the

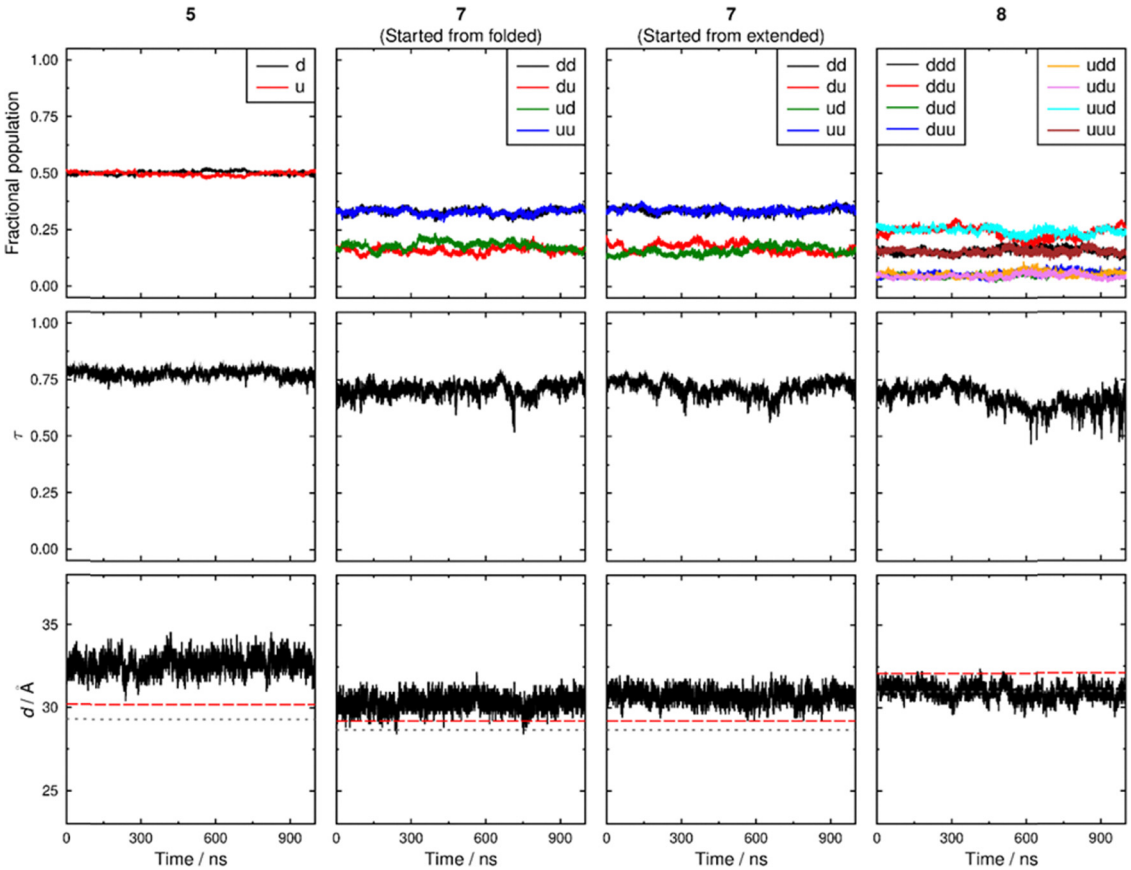

Fig. 10 Fractional populations of the general forms of **5**, **7** and **8** (top), positional order parameters, τ (middle) and layer spacings, d (bottom), all at 40 K below $T_{c,sim}$. The experimental layer spacings are shown at the equivalent experimental reduced temperature (dashed red line) and clearing point (dotted grey line).

Table 4 Fractional populations of the general forms of **5**, **7**, and **8** determined by averaging across the whole 1000 ns MD simulations run at 40 K below $T_{c,sim}$; the general forms that are related by a 180° rotation are paired

5		**7**			**8**	
			Started from folded[a]	Started from extended[a]		
d/u	49.8%/50.2%	dd/uu	33.0%/33.0%	33.5%/33.8%	ddd/uuu	15.7%/15.4%
		du/ud	15.9%/18.1%	16.9%/15.8%	ddu/uud	23.8%/24.5%
					dud/udu	5.0%/4.6%
					udd/duu	5.5%/5.6%

[a] Initial arrangement in which the system had started, prior to the pre-equilibrated runs at 40 K below $T_{c,sim}$ (details in the SI).

sugars, and that the alkyl chains (orange) form a wider layer between the sugar–triazole layers. The separate histograms for u and d molecules show that each ''full layer'' is made of two distinct sub-layers, one with the molecules pointing up and the other with the molecules pointing down. These sub-layers alternate along the z-axis of the simulation box, with the u and d head-groups and the u and d tail-groups, respectively, being interdigitated to some extent. The distance between the peaks in the total sugar populations is ≈32.2 Å (Table 5), which is less than twice the full length (≈48.8 Å) of the van der Waals surface of **5** with an all-*trans* alkyl chain (Table 3), and is consistent with the molecules being interdigitated (overlapped along their long axes) to some extent.

For each set of d or u molecules of **5**, the sugar population peaks have relatively narrow full-width-at-half-maximum (fwhm) values of ≈7.4 Å (Table 5), indicating a relatively narrow distribution of sugars within each sugar sub-layer. The sugar peaks of d and u molecules in the same layer are distinct from each other, with a separation of ≈5.1 Å between them (Table 5). The total sugar population peaks have a fwhm of ≈10.2 Å that is less than the sum of the fwhm values from a single pair of d and u sugars, such that the total sugar population histogram gives a single peak for each layer. These values and profiles are indicative of some interdigitation between the d and u sugar groups in the same layer, although they will overestimate the extent of local overlap because they arise from averaging across horizontal layers that are

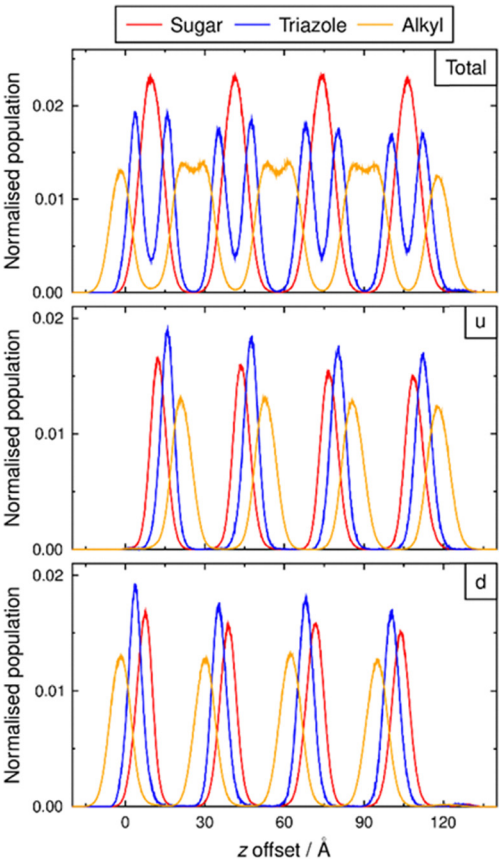

Fig. 11 Normalised populations of sugar (red), triazole (blue) and alkyl (orange) sets of atom centres, taken by averaging over 50–100 ns from the MD simulation of **5** at 40 K below $T_{c,sim}$, and showing atom sets from all of the molecules (top), and separately from the two different general forms (u and d).

not totally flat. The triazole population peaks from each set of d or u molecules are much wider than the length of a triazole group, indicating that their distribution within each triazole sub-layer is quite broad, and these triazole peaks have a separation for d and u molecules in the same layer that is consistent with the triazoles being positioned on either side of the sugar layer. The alkyl population peaks from each set of d or u molecules have relatively narrow fwhm values of ≈9.1 Å, which are significantly narrower than the distance of 11.51 Å between C1 and C10 atom centres in the DFT-optimised structure of the all-*trans* alkyl form of **5** shown in Fig. 5, and they are indicative of a relatively narrow alkyl distribution that may be attributed at least partly to the presence of conformers that are shorter than the all-*trans* alkyl form. The separation between the alkyl peaks of d and u molecules with chains in the same alkyl layer is comparable to the fwhm of each d and u peak and results in the double-peaked profile for the total alkyl populations. Additional analyses of the MD simulation showed that the all-*trans* alkyl form of **5** had a fractional population of only 1.4%, and that the average distance between the C1–C10 atom centres in the alkyl chain was 9.66 Å, with both values indicating that other (shorter) conformers are dominant. Together, these values and the double-peaked profile for the total alkyl populations are indicative of relatively limited overlap or interdigitation between the alkyl chains of d and u molecules of **5**. All of these results for **5** are reflected in the snapshots shown in Fig. 12, in which the left-hand snapshot shows whole d and u molecules, and the other snapshots show the sugars, triazoles and alkyl chains of the d and u molecules separately.

Systems that had initially been created from **7** in the folded form, which gave four layers, or **7** in the extended form, which gave eight layers, gave essentially the same results. The four-layer system gave simpler snapshots and population plots with slightly less noise due to having approximately twice the number of molecules in each layer as the eight-layer system. Hence, the results shown and discussed here are from the four-layer system, with the results from the eight-layer system given in the SI.

For **7**, the histogram of total populations given at the top of Fig. 13 is broadly similar to that of the total populations for **5** given at the top of Fig. 11, indicating that the overall phase structure is broadly similar. However, there are differences in the detail, as revealed by the separate histograms for the different general forms of **7**. The two folded forms (dd and uu) comprising ≈66% of the molecules in the lamellar phase of **7** show a very similar population distribution to that of the d and u molecules in the lamellar phase of **5**, forming two

Table 5 A selection of average separations between peaks and full-width-at-half-maximum values of peaks (in brackets), both in Å, from analyses of the MD simulation data at 50–100 ns for **5**, **7** and **8** at 40 K below the respective clearing points, shown in Fig. 11, 13 and 15

5				**7**				**8**			
Total	Sugar	32.2	(10.2)	Total	Sugar	30.5	(9.7)	Total	Sugar	31.0	(10.5)
	Triazole[a]	12.1	(6.7)		Triazole[a]	10.6	(7.6)		Triazole		
	Alkyl[b]	9.1	(17.8)		Alkyl[b]	9.6	(18.7)		Alkyl[b]		(20.1)
	Alkyl[a]	23.1	(17.8)		Alkyl[a]	20.9	(18.7)		Alkyl[a]		
d/u	Sugar[a]	5.1	(7.4)	dd/uu	Sugar[a]	5.7	(7.5)	ddd/uuu	Sugar[a]	8.1	(9.2)
	Triazole[a]	12.1	(6.6)		Triazole[a]	11.9	(7.3)				
	Alkyl[c]	9.1	(9.1)		Alkyl[c]	8.5	(9.4)				
				du/ud	Sugar[a]	<0.1	(7.8)	ddu/uud	Sugar[a]	0.8	(8.5)
					Triazole[a]	8.2	(7.2)				
					Alkyl[c]	8.5	(10.0)				
								dud/udu	Sugar[a]	3.4	(9.1)
								udd/duu	Sugar[a]	5.1	(9.6)

[a] Peaks in or across the same sugar layer. [b] Double-peaks across the full alkyl layer. [c] Peaks in the same alkyl layer.

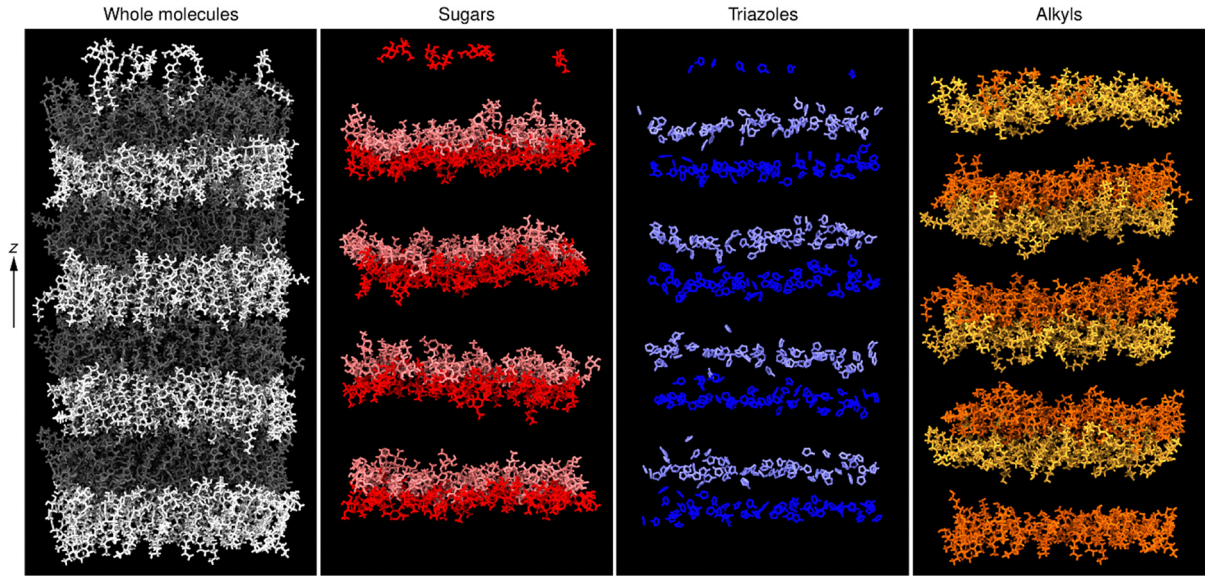

Fig. 12 Snapshots from the MD simulation of **5** at 40 K below $T_{c,sim}$, taken at 75 ns and rendering the same single frame in four different ways. From left to right: whole molecules d (white) and u (grey); the sugars of d (red) and u (light red); the triazoles of d (blue) and u (light blue); and the alkyl chains of d (orange) and u (light orange).

distinct sub-layers of dd and uu molecules that alternate along the *z*-axis of the simulation box. The two extended forms (du and ud) comprising ≈34% of the molecules in the lamellar phase of **7** give essentially identical population distributions to each other. Each population peak from the sugars of these extended molecules lies in the middle of the separate peaks from the two distinct sub-layers formed by the sugars of the folded molecules in the same layer. The triazoles of the extended molecules show a relatively broad distribution on either side of the sugars to which they are attached. The alkyl chains of the extended molecules have peaks between the sugar–triazole layers, while also showing a low-to-moderate population throughout the sugar–triazole layers. The distance between the peaks in the total sugar population is 30.5 Å, which is less than twice the full length (≈47.2 Å) of the van der Waals surface of **7** in the all-*trans*-alkyl folded form, less than the full length (≈42.6 Å) of the van der Waals surface of **7** in the all-*trans*-alkyl extended form, and less than the distance of 32.2 Å between the total sugar population peaks for **5**, and it is consistent with the molecules of **7** being interdigitated to some extent.

The positions of the folded (dd and uu) molecules of **7** and the extended (du and ud) molecules of **7** can be discussed initially as separate pairs.

For each set of dd or uu molecules of **7**, the sugar population peaks have fwhm values that are comparable to those for **5** (Table 5), and any overall differences from **5** are quite small, indicating that the folded molecules of **7** form a lamellar arrangement that is very similar to the lamellar phase structure of **5**. These results from the histograms are also reflected in the snapshots of the folded molecules of **7** shown in the top row of Fig. 14, which are comparable to the snapshots of **5** shown in Fig. 12.

The du and ud molecules of **7** give essentially the same peaks at the same positions as each other (averages within ≈0.05 Å), consistent with their equivalence by symmetry, and so their results can be considered as a single set. For the du and ud molecules, the sugar population peaks have relatively narrow fwhm values, indicating a distribution that is comparable to that of the folded forms (Table 5), but they are centred in the middle of the sugar layer, with their peaks lying between the two separate peaks from the sugars of the folded (dd and uu) forms. As a result of the structures and their relative positions, the triazole population peaks of the du and ud molecules lie closer to the centre of the sugar layers than the triazole peaks of the dd and uu molecules, indicating that they form a slightly separate set of triazole sub-layers. The alkyl population peaks of du and ud molecules have fwhm values that are broader than those for the folded forms of **7** and broader than those for **5**, which may be indicative of the alkyl chains adopting longer conformers in the extended form of **7**. The alkyl population peaks have a separation for extended molecules with chains in the same alkyl layer that is the same as that for the folded form of **7** and smaller than that for **5**. Overall, the extended molecules of **7** form a separate lamellar arrangement that is distinct from the lamellar arrangement of the folded molecules of **7** in the same phase, and from the lamellar phase structure of **5**. These results from the histograms of the extended molecules of **7** are also reflected in the snapshots shown in the bottom row of Fig. 14.

The histograms for the total populations, involving all the molecules of **7**, indicate that the total sugar layer of **7** is narrower that the total sugar layer of **5**, consistent with it being a contributory factor to the spacing between sugar layers being 1.7 Å shorter for **7** (30.5 Å) than **5** (32.2 Å) in these simulations. The triazole total population peaks for **7** have fwhm values that

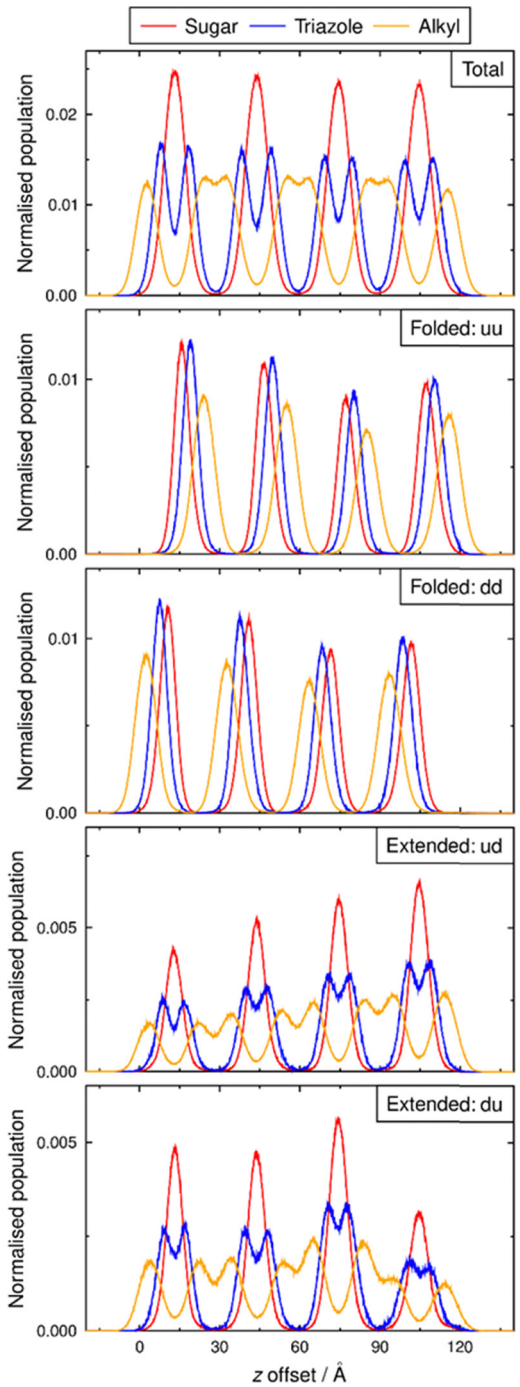

Fig. 13 Normalised populations of sugar (red), triazole (blue) and alkyl (orange) sets of atom centres, taken by averaging over 50–100 ns from the four-layer MD simulation of **7** at 40 K below $T_{c,sim}$, and showing atom sets from all of the molecules (top), and separately from the four different general forms.

are broader than those of **5**, indicative of a broader distribution within the triazole sub-layers of **7**, but a spacing between triazole peaks in the same layer of **7** that is shorter than that for **5**, indicating that the combined triazole-sugar layer is significantly narrower for **7** than **5**. The alkyl total population peaks for **7** have fwhm values across the full alkyl layer that are slightly broader those of **5**, and a spacing between peaks in the same alkyl layer that is greater than that for **5**. Additional analyses of the MD simulation showed that the alkyl chain of **7** had a fractional population of only 0.7% for the all-*trans* alkyl conformer, and an average alkyl C1–C10 atom centre distance of 9.47 and 9.52 Å for the folded and extended forms, respectively, which is significantly shorter than the average distance of 11.47 Å for each of the two chains in the DFT-optimised structure of the all-*trans*-alkyl folded form of **7** shown in Fig. 5. Together, these values indicate that the overall degree of alkyl chain interdigitation for **7** is limited, and broadly comparable to that for **5**. By contrast, the alkyl total population peaks have a spacing of ≈20.9 Å between alkyls either side of the same sugar layer of **7** that is ≈2.2 Å narrower than that for **5**. Hence, the results suggest that both a narrower sugar–triazole layer and a narrower alkyl layer arising from the positioning of all the alkyl groups from both forms of **7** are together responsible for the layer spacing being narrower in the lamellar phase of **7** than the lamellar phase of **5**.

The snapshot at the bottom left of Fig. 14 shows a representation of all the molecules of **7**, and illustrates how the extended molecules are interwoven and dispersed among the folded molecules, both laterally and vertically. A combination of the histograms and all the snapshots suggests that the lamellar phase of **7** might be considered to consist of two contiguous sub-phases. One sub-phase comprises folded molecules of **7** that form two distinct sub-layers within each of the "full layers", similar to the lamellar phase structure of **5**. The other sub-phase comprises extended molecules of **7** that form a more continuous system of "full layers" that sit within and to some extent bridge the sub-layers of the folded molecules. Each sub-phase involves interdigitation of the respective tail-groups to some extent, and also of the sugar head-groups for the folded form of **7**. The ratio of folded to extended molecules in the lamellar phase of **7** is approximately 2 : 1, which equates to a pair of folded molecules accompanying each extended molecule within a notional uu/ud/dd unit, although such distinct units are not observed as consistent features in the highly fluid phases present in the simulations.

For **8**, the histogram of total populations at the top of Fig. 15 shows distinct sugar, triazole and alkyl layers that have a general similarity to those for **5** and **7**. The moderate triazole and alkyl populations within the sugar layers of **8** are more comparable to those of **7** than **5**, and from this perspective the lamellar phase of **8** appears broadly similar to that of **7**.

The forms of **8** with one alkyl chain pointing in the opposite direction to the other two alkyl chains give individual plots with asymmetric triazole and alkyl populations, consistent with these structures, and the equivalent pairs of forms (ddu/udd, dud/udu, udd/duu) give profiles that are mirror images of each other, consistent with the symmetry of the paired forms. The individual forms with low fractional populations of ≈4–6% (dud, udu, udd and duu) give more variable histograms within the 50 ns time-window, resulting from the presence of only ≈20–30 molecules dispersed across eight layers. For **8**, the eight general forms can be discussed initially as four separate pairs.

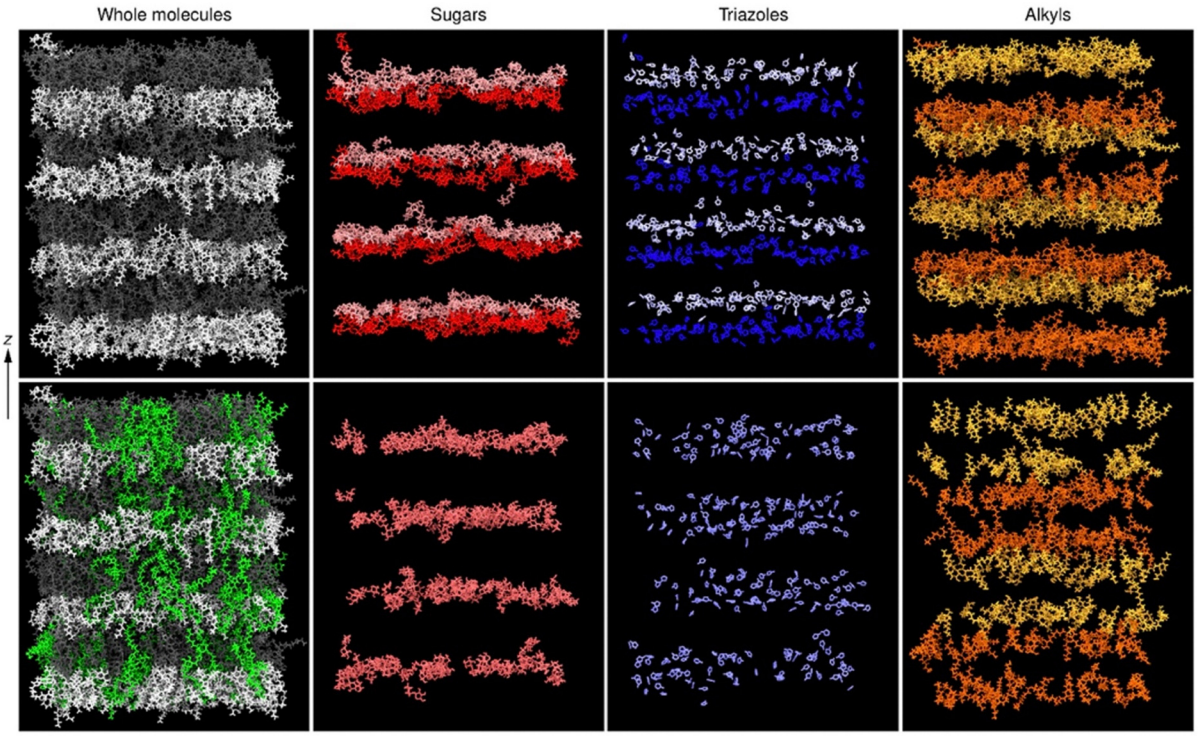

Fig. 14 Snapshots from the four-layer MD simulation of **7** at 40 K below $T_{c,sim}$, taken at 87.6 ns and rendering the same single frame in eight different ways. The top row shows only dd and uu molecules, with du and ud molecules omitted, and from left to right: whole molecules dd (white) and uu (grey); the sugars of dd (red) and uu (light red); the triazoles of dd (blue) and uu (light blue); and the alkyl chains of dd (orange) and uu (light orange). The bottom row shows du and ud molecules (in the same colour because they are equivalent), and from left to right: whole molecules of du and ud (green) added to the image in the row above, so that all the molecules in the frame are shown; the sugars of only du and ud (medium red); the triazoles of only du and ud (medium blue); and the alkyl chains of only du and ud, in this case colour-coded so that both alkyl chains of each du and ud molecule with a sugar in the same layer are either orange or light orange for alternate layers, to illustrate the limited extent of interdigitation in the alkyl layer.

The two fully folded forms (ddd and uuu) comprising ≈31% of the lamellar phase of **8** form two distinct sub-layers that are comparable to the sub-layers formed by the single-chain molecules (d and u) comprising 100% of the lamellar phase of **5**, and the folded forms (dd and uu) comprising ≈66% of the lamellar phase of **7**. These results are reflected in the snapshots of the ddd and uuu molecules of **8** shown in Fig. 16 (top left of each cluster of four snapshots).

The two partially folded forms of **8** where chains 1 and 2 point in similar directions (ddu and uud) comprising ≈48% of the phase, have sugar population peaks that lie between the ddd and uuu sugar peaks, indicating that the sugars of these ddu and uud forms occupy the middle of the sugar layers for **8**, which is comparable to the positioning of the sugars of the extended molecules in the sugar layers of **7**. However, whereas the sugars of the two forms of the extended molecule of **7** (du and ud) have identical population peaks that lie at the centre of the sugar layer, the sugars of the ddu and uud forms of **8** give peaks that are offset by ≈0.8 Å from each other, such that they form two distinct sub-layers. These sub-layers are distinct but are very close to each other and are strongly overlapped. This small offset between the sugars of the ddu and uud forms results in the side of the molecule with two alkyl groups being slightly closer to their associated alkyl layer, and the side of the molecule with only one alkyl group slightly further away from its associated alkyl layer. These results are reflected in the snapshots of the ddu and uud molecules of **8** shown in Fig. 16 (top right of each cluster of four snapshots).

The two other pairs of partially folded forms of **8** show sugar population peaks that are offset from each other for the dud and udu pair that comprises ≈10% of the lamellar phase, and for the udd and duu pair that comprises ≈11% of the lamellar phase. Hence, these two other pairs show population distributions that are distinct from each other, and intermediate between those for the two dominant pairs of forms of **8**. As with the ddu/uud pair, the offset for these two other pairs results in the side of the molecule with two alkyl groups being closer to their associated alkyl layer. The results are reflected to some extent in the snapshots of these pairs shown in Fig. 16 (bottom pair of each cluster of four snapshots) but they are less discernible because of the relatively small numbers of these forms of the molecule in the simulation.

The peaks in the total sugar population of **8** are slightly broader than those of **7** and **5**, and have a separation between these total sugar population peaks of ≈31.0 Å for **8** that is slightly larger than that of ≈30.5 Å for **7** and smaller than that of ≈32.2 Å for **5**. The overall results are consistent with various degrees of interdigitation between the respective head- and tail-

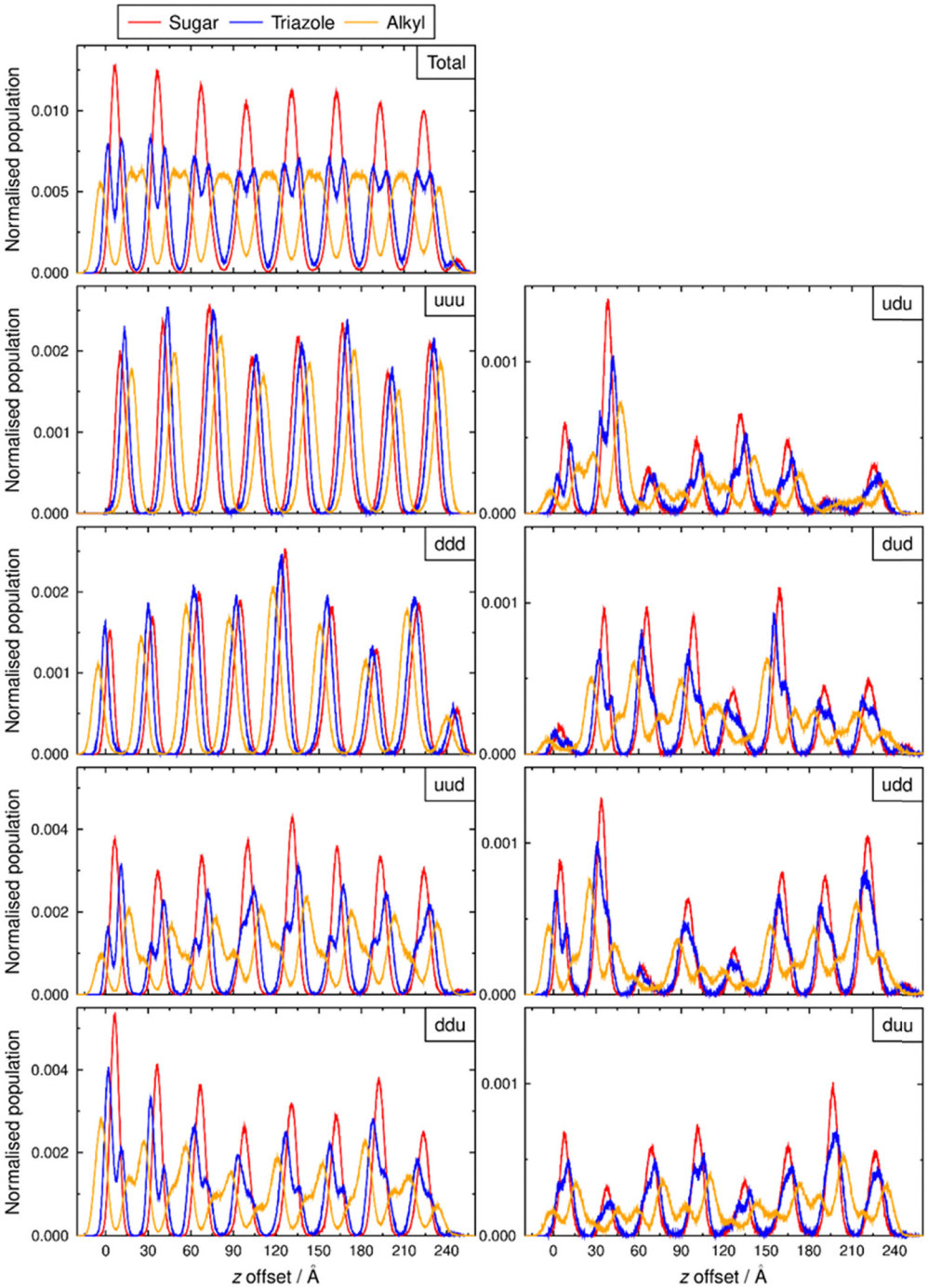

Fig. 15 Normalised populations of sugar (red), triazole (blue) and alkyl (orange) sets of atoms centres, taken by averaging over 50–100 ns from the four-layer MD simulation of **8** at 40 K below $T_{c,sim}$, and showing atom sets from all of the molecules (top), and separately from the eight different general forms.

groups of the various forms of **8**. Together, the results from the histograms and the snapshots suggest that the lamellar phase of **8** might be considered to consist of four contiguous sub-phases, arising from the four pairs of forms self-organising into distinct sets of sub-layers. For **8**, three pairs of forms are positioned in a way that is similar to the folded molecules of **7**, whereas the ddu/udd pair is positioned in a way that is more comparable to the extended molecules of **7**. The ratio of these "more folded" to "quasi-extended" molecules in the lamellar phase of **8** is close to 1 : 1, *versus* the 2 : 1 ratio in the lamellar phase of **7**, and this difference may result partly from the "quasi-extended" molecules of the trisaccharide **8** being inherently asymmetric *versus* the more symmetric extended forms of the disaccharide **7**.

Overview of the phase structures from the MD simulations. The MD simulations seem to provide a plausible basis for

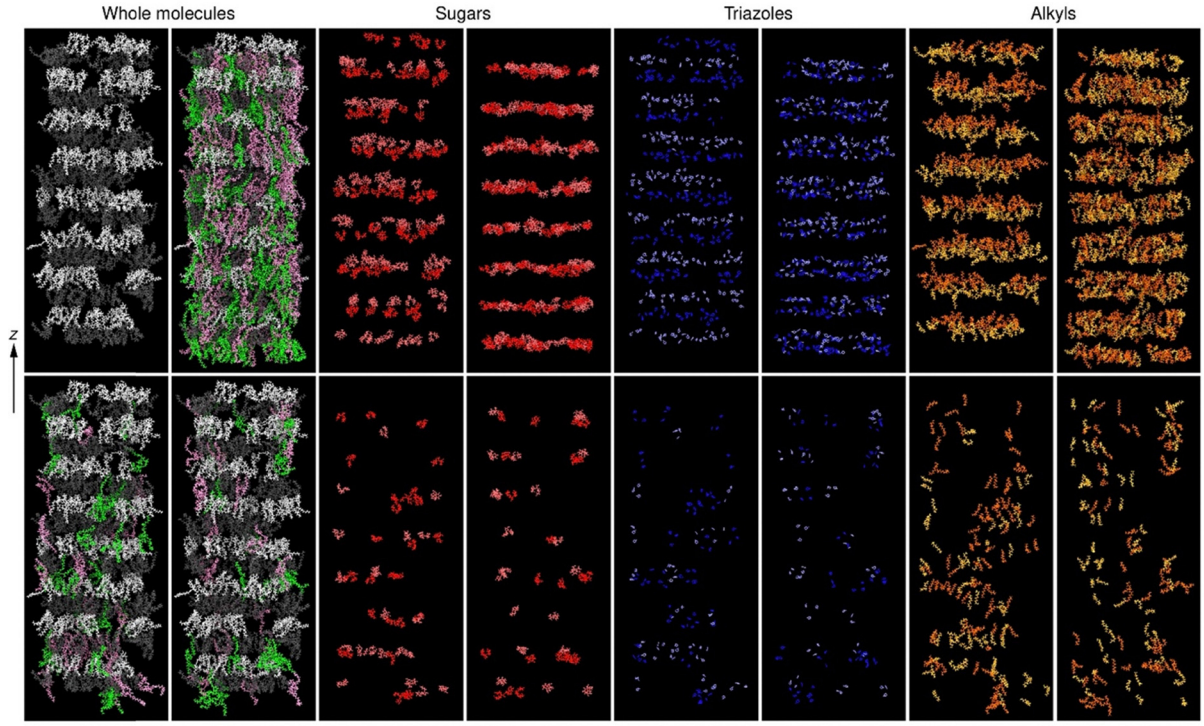

Fig. 16 Snapshots from the MD simulation of **8** at 40 K below $T_{c,sim}$, taken at 89.6 ns and rendering the same single frame in sixteen different ways. Each cluster of four snapshots shows ddd/uuu (top left), ddu/udd (top right), dud/udu (bottom left) and udd/duu (bottom right) molecules. From left to right, the clusters show: whole molecules, only sugars, only triazoles, and only alkyl chains. The top left whole molecule snapshot shows only ddd/uuu molecules as white/grey, with the other three whole molecule snapshots also including either ddu/udd, dud/udu or udd/duu molecules, respectively, each as green/violet. The snapshots of only sugars, triazoles and alkyls chains show ddd/uuu, ddu/uud, dud/udu and udd/duu as red/light red, blue/light blue and orange/light orange, respectively.

interpreting the overall experimental results, albeit with the caveat that the clearing points in the MD simulations are significantly higher than the experimental values and the temperatures at which the simulations were run may not provide a good match for close quantitative comparisons with experimental data. The simulations indicate that the monosaccharide **5** gives a relatively simple lamellar phase structure that provides a basis from which to consider the more complex phase structures indicated for disaccharide **7** and trisaccharide **8**.

For **5**, the layer spacing of 32.2 Å from the simulation at 40 K below the clearing point is greater than that of ≈29.3 Å observed just below the clearing point experimentally (Fig. 7), and an extrapolation of the temperature-dependent experimental data suggests such a layer spacing might occur at ≈130 K below the clearing point if the phase were maintained experimentally in that region. The simulations of the lamellar phase showed strong inter- and intramolecular interactions involving the polar head-groups of **5**, which packed together in distinct sub-layers. The relatively small enthalpy change observed experimentally at the clearing point of **5** (Table 2) suggests that strong interactions are likely to be maintained between head-groups in the isotropic phase, and the relatively small experimental entropy change at the clearing point (Table 2) suggests that the gain in positional freedom on going to the isotropic phase may be relatively small. Both aspects are consistent with the strong interactions and limited motional freedom seen in simulations we carried out on **5** in the isotropic phase at a temperature above the clearing point in the simulations.

For **7**, the layer spacing of 30.5 Å from the simulation at 40 K below the clearing point is similar to that of ≈29.3 Å observed experimentally at 40 K below the clearing point, and this layer spacing shows only a weak temperature dependence experimentally (Fig. 7). As discussed above, close inspection reveals that a narrower sugar–triazole layer and a narrower alkyl layer arising from a greater degree of interdigitation are responsible for the layer spacing being narrower for **7** than **5**. The enthalpy change observed experimentally at the clearing point of **7** is × 2.28 greater than that observed for **5**, which suggests that the introduction of the extended molecules with their sugar–triazole groups in the middle of the sugar layers may have increased the strength of the polar interactions in the lamellar phase of **7** relative to those of **5**, consistent with the narrower layer spacing for **7**. The experimental entropy change at the clearing point of **7** is × 1.81 greater than that of **5**, indicating that the gain in positional freedom on going from the lamellar to isotropic phase is greater for **7** than **5**, which seems consistent with a more complex self-organised lamellar phase structure for **7** than **5**. The higher experimental clearing point for **7** than **5** results from the greater relative increase in ΔH than

ΔS at the clearing point ($\times$2.28 *versus* $\times$1.81) on going to **7** from **5**, which in turn may be attributable primarily to the stronger interactions within the polar sugar–triazole layers of **7** *versus* **5**.

For **8**, the layer spacing of 31.0 Å from the simulation at 40 K below the clearing point is similar to that of 31.9 Å observed experimentally (Fig. 7). As discussed above, close inspection reveals that a broad sugar–triazole layer and a broad alkyl layer, along with interdigitation of the respective head- and tail-groups of the various forms of **8**, contribute to the layer spacing for **8** being intermediate between than for **7** and **5**. Overall, the greater number of sugar, triazole and alkyl groups per molecule, and the way that the different general forms of the molecule self-organise, result in a more complex phase structure for **8** than for **7** or **5**. The enthalpy change observed experimentally at the clearing point of **8** is $\times$1.54 greater than that observed for **5**, which suggests that the polar interactions in the sugar–triazole layer have increased relative to those of **5**. The experimental change in the entropy at the clearing point of **8** is $\times$1.35 greater than that of **5**, indicating that the gain in positional freedom on going from the lamellar to isotropic phase is greater for **8** than **5**, which is consistent with the more complex self-organised phase structure of **8**. Both of these increases for **8** *versus* **5** are smaller than those of $\times$2.28 and $\times$1.81, respectively, for **7** *versus* **5**, and the experimental clearing point of **8** lies between those of **7** and **5**. It seems reasonable to attribute these relative values to the polar interactions within the sugar–triazole layers and the self-organisation in the lamellar phase *versus* the isotropic phase being particularly favourable for disaccharide **7** in comparison with monosaccharide **5**, and with trisaccharide **8** having intermediate behaviour.

3.5 Relation to the phases of other glycolipids more generally

The series of mono-, di- and tri-saccharides, **5**, **7** and **8**, studied here all exhibit only lamellar mesophases with phase structures that are broadly comparable with each other. By contrast, earlier studies of an analogous series of mono-, di-, and tri-*O*-β-D-galactopyranosyl-*O*-alkyl pentaerythritols, see Fig. 17, found that they exhibited distinctly different mesophases to each other, with the monosaccharide (**9**) exhibiting a columnar phase, the disaccharide (**10**) a lamellar (SmA) phase, and the trisaccharide (**11**) a cubic phase.[30,31] There are important contrasts between the molecular architectures of these two analogous families of materials, which affect the natures of the mesophases formed; these appear to lie in molecular shape, flexibility, and hydrophilic/hydrophobic balance.

For example, the α-D-glucopyranosides (**5** to **8**) have triazole ring units attached to the saccharide moieties that provide a degree of internal rigidity and an extension to the molecular architectures. Whereas, for the other family of materials (**9** to **11**), the saccharides are attached to the pentaerythritol parts, which allow for more flexibility associated with the internal linkages or segments. The stiffer internal molecular architectures support the formation of rod-like architectures for the glucopyranosides, as indicated in the molecular models in Fig. 5, whereas the flexibility in the pentaerythritols allows for the minimization of the free volumes of the molecular architectures to be rod-like, wedge-like, or spherical. The packing together of molecules with these shapes as a function of hydrophilic/hydrophobic balance, consequently, induces curvature into the local packing of the molecules that in turn affects the types of mesophases formed. This is reflected across the family of pentaerythritol compounds, which all exhibit thermotropic mesophases, but not necessarily with all possessing the same mesophase type, as seen in Fig. 17. One detail that affects mesophase properties is the number of hydroxyl components in the molecular structure of a material, with the material having the largest proportion of H-bonding units having the higher clearing point; whereas, in comparison, the material with the largest proportion of aliphatic chains has the lowest.

The comparisons of the results and observed properties serve to demonstrate that materials **9** to **11** have more flexible structures than those of materials **5** to **8** that are under examination in this article. And moreover, the differences

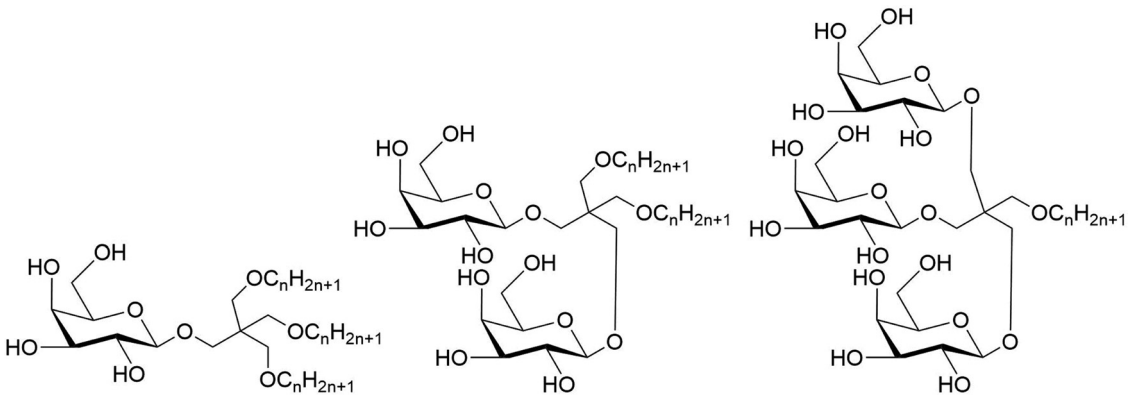

Fig. 17 Liquid-crystalline materials based on mono- (**9**), di- (**10**) and tri- (**11**) *O*-alkyl pentaerythritol derivatives having mono, di- or tri-galactosyl head groups, along with the phase sequences for the materials with n = 12 (temperatures in °C).

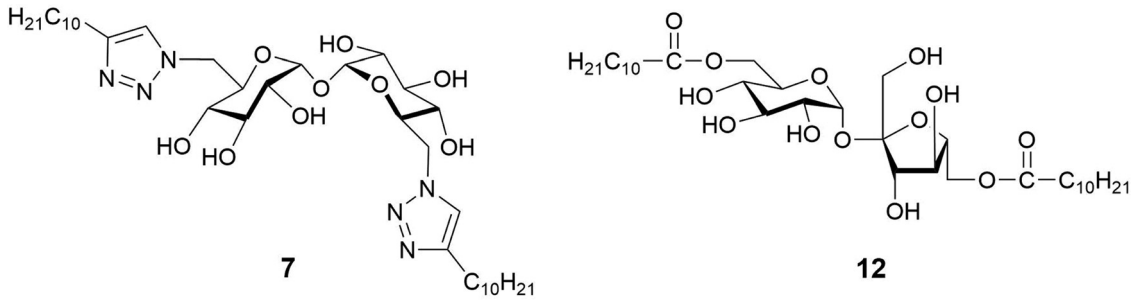

Fig. 18 Comparison between the temperatures (°C) of the phase transitions of compound **7** and 6,6′-di-*O*-undecanoylsucrose **12**.

between the two families are likely to be focused on the triazole ring system, which appears to support the formation of lamellar phases.

A further comparison can be made between the two rod-like materials shown in Fig. 18; compound 7 is taken from the present studies, and 6,6′-di-*O*-undecanoylsucrose **12** was reported previously.[32] Compounds 7 and **12** possess the same aliphatic chain lengths, and the same hydroxyl content associated with the central carbohydrate core units. As expected, the melting and clearing points of the triazole **7** are substantially higher than those of the sucrose derivative **12** (*i.e.*, 28 and 45 °C higher, respectively). The result shows that the incorporation of the triazole moieties in effect extends the relative molecular lengths and increases the rigidity, thereby stabilizing the lamellar (SmA) phase, as we see for the family series of molecules **5** to **8**. Interestingly, the 6,6′-di-*O*-undecanoylsucrose was also predicted, and found, to have both folded and interdigitated molecular architectures located within the structure of the lamellar phase.[32] In this comparison it appears that these molecules with softer internal molecular architectures can also form folded and interdigitated packing arrangements similar to those molecules that have more extended and rigid structures. Furthermore, it appears that compounds of type 7 and **12** have common pretransitional effects occurring in the liquid above the clearing points as shown by X-ray diffraction studies.

4. Conclusion

Overall, the experimental studies of the mono- di- and trisaccharides, **5**, **7** and **8**, using POM, DSC and X-ray diffraction, along with DFT calculations and MD simulations provide a coherent view of their mesophase structures, along with general consistency with a wider view of the dependence of glycolipid phase behaviour on molecular architecture. Examining the two families of materials (**5** to **7**) and (**9** to **12**), the amphiphiles with two aliphatic chains appear to give the most stable mesogens with the widest smectic ranges, high clearing points, the least dependency on temperature, and the possibility of exhibiting folded molecular structures. It may be that this combination of artifacts is why so many natural membrane lipids, such as glyco- and phospho-lipids, have molecular structures composed of a head group with two aliphatic chains of substantial length (10 to 20 methylene units),[7,8] thereby resulting in overall conformationally flexible architectures.

Disclosure statement

No potential conflict of interest was reported by the authors.

Conflicts of interest

There are no conflicts to declare.

Data availability

Data from this article relating to the MD simulations and SAXS experiments is available by request from the University of York Data Catalogue. DOI: **https://doi.org/10.15124/86717a02-5019-40e3-89b6-41aa19882cd4.**

Supplementary information contains experimental procedures and associated spectral analyses, X-ray diffraction data and details of computational methodologies. See DOI: **https://doi.org/10.1039/d5sm00640f**.

Acknowledgements

Financial support from CNRS and MESRI is gratefully acknowledged. The authors also thank SEPPIC and CNRS for grant to Céline Besset. The authors are also indebted to financial support from the EPSRC (Platform grant EP/D055261/1, Core Capability grant EP/K039660/1, and Standard grant EP/M020584/1). We are grateful to Dr R. J. Mandle for his technical contributions to our initial molecular simulations. The authors acknowledge also the support from the colleagues responsible for the analytical facilities (Centre de Spectrométrie de Masse and Centre Commun de Resonance Magnétique Nucléaire of the University Claude Bernard).

References

1 P. J. Collings and J. W. Goodby, *Introduction to Liquid Crystals*, CRC Press (T&F), Boca-Ratan, Florida, USA, 2019, ISBN 978-1-138-29876.

2 R. Virchow, *Virchows Archiv Pathol. Anantomie u. Physiol. Bd.*, 1854, **6**, 562–4572.
3 F. Reinitzer, *Monatshefte*, 1888, **9**, 421–441.
4 J. L. Fergason, *Appl. Optics*, 1963, **7**, 91.
5 B. Boettcher, *Materialsprufung*, 1969, **11**, 156.
6 J. L. Fergason, *Sci. Am.*, 1964, **211**, 77.
7 G. H. Brown and J. J. Wolken, *Liquid Crystals and Biological Structures*, Academic Press, London, 1979.
8 O. G. Mouritsen, Life as a Matter of Fat, *The Emerging Science of Lipidomics*, Springer-Verlag, Heidelberg, 2005.
9 G. T. Stewart, *Liq. Cryst.*, 2003, **30**, 541–557.
10 Z. Yang, R. Xu, S. Chambert, L. Soulère, M. Ahmar, G. Mackenzie, S. J. Cowling, J. W. Goodby and Y. Queneau, in *Carbohydrate Chemistry*, ed. A. P. Rauter, T. Lindhorst and Y. Queneau, RSC Special Periodic Reports, Cambridge, UK, 2017, vol. 42, pp. 274–312.
11 D. M. Small, *J. Colloid Interface Sci.*, 1977, **58**, 581.
12 W. L. Porter, *Am. Potato J.*, 1972, **49**, 403–437.
13 V. Grassert and V. Vill, *Liq. Cryst. Today*, 1994, **4**, 4–5.
14 J. P. Dworkin, D. W. Deamer, S. A. Sandford and L. J. Allamandola, *Proc. Natl. Acad. Sci. U. S. A.*, 2001, **98**, 815–819.
15 D. Segré, D. Ben-Eli, D. W. Deamer and D. Lancet, The Lipid World, *Orig. Life Evol. Biosph.*, 2001, **31**, 119–145.
16 G. W. Gray and J. W. Goodby, *Smectic Liquid Crystals – Textures and Structures*, Leonard Hill, Glasgow and London, 1984, ISBN: 0-249-44168-3.
17 S. J. Cowling, Optical Microscopy Studies of Liquid Crystals, in *the Handbook of Liquid Crystals Vol 1: Fundamentals of Liquid Crystals*, ed. J. W. Goodby, P. J. Collings, T. Kato, C. Tschierske, H. F. Gleeson and P. Raynes, Wiley-VCH, Weinheim, 2014, ch. 9, pp. 263–300.
18 J. W. Goodby, Phase Transitions: General and Fundamental Aspects, in *The Handbook of Liquid Crystals Vol 1: Fundamentals of Liquid Crystals*, ed. J. W. Goodby, P. J. Collings, T. Kato, C. Tschierske, H. F. Gleeson and P. Raynes, Wiley-VCH, Weinheim, 2014, ch. 3, pp. 59–76.
19 D. M. Agra-Kooijman and S. Kumar, X-ray Scattering Investigations of Liquid Crystals, in *The Handbook of Liquid Crystals Vol 1: Fundamentals of Liquid Crystals*, ed. J. W. Goodby, P. J. Collings, T. Kato, C. Tschierske, H. F. Gleeson and P. Raynes, Wiley-VCH, Weinheim, 2014, ch. 10, pp. 300–338.
20 C. Besset, S. Chambert, B. Fenet and Y. Queneau, *Tetrahedron Lett.*, 2009, **50**, 7043–7047.
21 C. W. Tornøe, C. Christensen and M. J. Meldal, *Org. Chem.*, 2002, **67**, 3057–3064.
22 M. Meldal and C. W. Tornøe, *Chem. Rev.*, 2008, **108**, 2952–3015.
23 V. K. Tiwari, B. B. Mishra, K. B. Mishra, N. Mishra, A. S. Singh and X. Chen, *Chem. Rev.*, 2016, **116**, 3086–3240.
24 K. Singh, R. Tyagi, V. K. Mishra, G. Tiwari and R. Sagar, *SynOpen*, 2023, **7**, 322–352.
25 V. Molinier, B. Fenet, J. Fittremann, A. Bouchu and Y. Queneau, *J. Colloid Interface Sci.*, 2005, **286**, 360–368.
26 V. Maunier, P. Boullanger, D. Lafont and Y. Chevalier, *Carbohydr. Res.*, 1997, **299**, 49–57.
27 N. H. Hartshorne and A. Stuart, *Crystals and the Polarizing Microscope*, 4th edn, Edward Arnold, London, 1970, SBN: 7131 2256 0.
28 M.-S. Ho and C.-S. Hsu, *Liq. Cryst.*, 2010, **37**, 293–301.
29 M. J. Frisch, G. W. Trucks, H. B. Schlegel, G. E. Scuseria, M. A. Robb, J. R. Cheeseman, G. Scalmani, V. Barone, G. A. Petersson, H. Nakatsuji, X. Li, M. Caricato, A. V. Marenich, J. Bloino, B. G. Janesko, R. Gomperts, B. Mennucci, H. P. Hratchian, J. V. Ortiz, A. F. Izmaylov, J. L. Sonnenberg, D. Williams-Young, F. Ding, F. Lipparini, F. Egidi, J. Goings, B. Peng, A. Petrone, T. Henderson, D. Ranasinghe, V. G. Zakrzewski, J. Gao, N. Rega, G. Zheng, W. Liang, M. Hada, M. Ehara, K. Toyota, R. Fukuda, J. Hasegawa, M. Ishida, T. Nakajima, Y. Honda, O. Kitao, H. Nakai, T. Vreven, K. Throssell, J. A. Montgomery Jr., J. E. Peralta, F. Ogliaro, M. J. Bearpark, J. J. Heyd, E. N. Brothers, K. N. Kudin, V. N. Staroverov, T. A. Keith, R. Kobayashi, J. Normand, K. Raghavachari, A. P. Rendell, J. C. Burant, S. S. Iyengar, J. Tomasi, M. Cossi, J. M. Millam, M. Klene, C. Adamo, R. Cammi, J. W. Ochterski, R. L. Martin, K. Morokuma, O. Farkas, J. B. Foresman and D. J. Fox, *Gaussian 16, Revision A.03*, Gaussian, Inc., Wallingford CT, 2016.
30 F. Dumoulin, D. Lafont, T.-L. Huynh, P. Boullanger, G. Mackenzie, J. J. West and J. W. Goodby, *Chem. – Eur. J.*, 2007, **13**, 5585–5600.
31 J. W. Goodby, V. Görtz, S. J. Cowling, G. Mackenzie, P. Martin, D. Plusquellec, T. Benvegnu, P. Boullanger, D. Lafont, Y. Queneau, S. Chambert and J. Fitremann, *Chem. Soc. Rev.*, 2007, **36**, 1971–2032.
32 V. Molinier, P. H. J. Kouwer, J. Fitremann, A. Bouchu, G. Mackenzie, Y. Queneau and J. W. Goodby, *Chem. – Eur. J.*, 2007, **13**, 1763–1775.